arXiv:cond-mat/0007510v1 [cond-mat.supr-con] 31 Jul 2000

Angular-dependence of the penetration depth in unconventional superconductors

Klaus Halterman* and Oriol T. Valls†
School of Physics and Astronomy and Minnesota Supercomputer Institute
University of Minnesota
Minneapolis, Minnesota 55455-0149

Igor Žutić‡
Department of Physics and Center for Superconductivity Research
University of Maryland
College Park, Maryland 20742

(February 1, 2008)

We examine the Meissner state nonlinear electrodynamic effects on the field and angular dependence of the low temperature penetration depth, λ, of superconductors in several kinds of unconventional pairing states, with nodes or deep minima ("quasinodes") in the energy gap. Our calculations are prompted by the fact that, for typical unconventional superconducting material parameters, the predicted size of these effects for λ exceeds the available experimental precision for this quantity by a much larger factor than for others. We obtain expressions for the nonlinear component of the penetration depth, $\Delta\lambda$, for different two- and three- dimensional nodal or quasinodal structures. Each case has a characteristic signature as to its dependence on the size and orientation of the applied magnetic field. This shows that $\Delta\lambda$ measurements can be used to elucidate the nodal or quasinodal structure of the energy gap. For nodal lines we find that $\Delta\lambda$ is linear in the applied field, while the dependence is quadratic for point nodes. For layered materials with $YBa_2Cu_3O_{7-\delta}$ (YBCO) type anisotropy, our results for the angular dependence of $\Delta\lambda$ differ greatly from those for tetragonal materials and are in agreement with experiment. For the two- and three- dimensional quasinodal cases, $\Delta\lambda$ is no longer proportional to a power of the field and the field and angular dependences are not separable, with a suppression of the overall signal as the node is filled in.

72.40.Hi,74.25.Nf,74.20.De

I. INTRODUCTION

Until about fifteen years ago, the question of the determination of pairing states in superconductors was one of small and purely theoretical interest, since no existing superconductors were commonly suspected[1] to be in a state other than the standard *s*-wave. Only liquid ^{3}He was known[2] to exhibit *p*-wave pairing in its several superfluid phases. Since then, the situation has dramatically changed. First, extensive studies in high temperature oxide superconductors (HTSC's) have led to the widespread belief[3] that in most cases the order parameter for these materials is at least predominantly *d*-wave, with lines of nodes in a quasi two-dimensional Fermi surface (FS). Whether these are true nodes or very deep minima is, however, not really established even in the best studied compounds[4], and the situation is less clear in some[5,6] other cases. More recently, unconventional pairing states have been proposed, on evidence of varying strength, for a plethora of other materials with lower superconducting transition temperatures. Among these materials are some heavy fermion (HF) compounds[7–10], members[11–16] of certain superconducting families of organic salts such as $\kappa-(\mathrm{BEDT-TTF})_2\mathrm{Cu(NCS)}_2$ and $(\mathrm{TMTSF})_2\mathrm{X}$ ($\mathrm{X}=\mathrm{PF}_6, \mathrm{ClO}_4$, etc.), and certain other salts such as[17–21] Sr_2RuO_4 for which a pairing state similar to that in the A-phase of ^{3}He has been[22–25] suggested, although recently other states[26] have also gained favor.

To probe the *bulk* order parameter (OP) it is best to use experimental techniques that measure properties over a scale of the penetration depth[27] λ, which in most materials of interest, as mentioned above, is much larger than the coherence length ξ. The OP at the surface may differ from that in the bulk, and furthermore, surface experiments are subject to uncertainties arising from surface quality and preparation problems. In cases where the OP leads to an energy gap which has nodes (or very deep minima which we denote as "quasinodes"), it was pointed out eight years[28] ago, that excitation of quasiparticles near the nodes by an applied magnetic field leads to nonlinear anisotropies[29–33] in the electromagnetic properties of the material. It was shown[34] that one can in principle use these anisotropies to perform "node spectroscopy", that is, not only to detect the existence of nodes (or quasinodes) but to infer their location on the FS.

Although in the earliest work[28,29] anisotropies in the penetration depth were considered possible subjects of experimental investigation, emphasis soon switched to related quantities, chiefly the anisotropic component of the magnetic moment *transverse* to the applied field, and the torque associated with it. This quantity seemed more accessible experimentally than λ, which was deemed to be more difficult to measure with the requisite precision. However, recent advances and refinements in experimental techniques force a reconsideration of this assessment. The best measurements[35] of the transverse magnetic moment yield only a relatively weak lower bound on the magnitude of the gap at a quasinode, because the noise of the measurements is relatively high, with a resulting uncertainty a factor of only three below the maximum signal expected for a system with pure nodes. On the other hand, measurements of the penetration depth in compounds such as YBCO can now be performed[36] with a precision of a small fraction of an Ångstrom. As we show later, this is one or two orders of magnitude below the putative signal for that compound. Furthermore[37], for many of the non-HTSC compounds mentioned above, the predicted nonlinear signal can be considerably larger than that expected for HTSC's. Hence, extension of techniques such as those of Ref. 36 to dilution refrigeration temperatures is likely to allow the determination of the nodal structure of these materials. It appears, therefore, that measurements of λ are the most promising way of probing the nodal structure of the gap through nonlinear electromagnetic effects.

With this in mind, we discuss here the nodal spectroscopy of the penetration depth. We define the quantity $\Delta\lambda(\psi) \equiv \lambda(\psi, H_A) - \lambda(\psi, 0)$ where H_A is the magnitude of the applied field and ψ the angle it forms with a suitably defined axis. In defining $\lambda(\psi, H_A)$ attention must be paid to the experimental methods involved. We then present results that show that the field and angular dependence of $\Delta\lambda(\psi)$ will reflect the nodal or quasinodal structure of the energy gap. We first consider quasi two-dimensional sytems with *d*-wave pairing. In this case, we show that the orthorhombicity as it occurs in compounds of the YBCO type, must be included in a proper and clear way. We calculate the necessary fields and find that the effects of orthorhombicity in $\Delta\lambda(\psi)$ are very important, and that their neglect has led to misleading conclusions in interpreting experiments. We then turn to other quasi two-dimensional nodal and quasinodal cases, for which the required results are readily obtained from previously published field distributions.[34] Finally, we consider three dimensional systems with point or line nodal[37] structures with quasinodal admixtures. In our conclusions, we point out that the penetration depth can indeed be used to perform node spectroscopy in all these cases and elaborate on the use of our results to interpret existing or future experiments.

II. METHODS

A. Penetration depth

As explained above, our focus is on the angular dependence of the penetration depth λ, as a very powerful probe in the understanding of the symmetry of the bulk OP for unconventional superconductors. The presence of nodes or quasinodes in the energy gap gives rise[28,34] to nonlinear corrections in the current response to an applied magnetic field, $\mathbf{H}_\mathrm{A}$. These nonlinear corrections result in λ having an angular and field dependence that reflects directly the symmetry of the pairing state.

The first question we must address is that of defining the angular dependent penetration depth in the nonlinear case. This involves both theoretical and experimental difficulties. Let us consider the geometry of a semi-infinite superconducting slab of thickness d, much larger than any relevant penetration depth. The slab is oriented perpendicular to one of the symmetry axes, e.g., the c axis, and assuming orthorhombic or higher symmetry, its surfaces are parallel to the plane spanned by the other two (e.g. the a and b) axes. This is the geometry that we will consider in this work. In the linear case, the penetration depth is described in terms[38] of the superfluid density tensor, and its principal axes are those of symmetry. The principal values λ_a and λ_b can be determined by experiments involving an applied field along the b and a directions, respectively. Thus one can use, for example, as a conventional[39] definition, $\lambda_i \equiv \int_0^\infty \mathrm{d}z H_j(z)/H(0)$, where $H_j(z)$ is the magnetic field along a principal axis, which depends exponentially on the distance z within the sample through only one of the principal values. Alternatively, one can write λ_i in terms of the spatial derivatives of the fields at the surface, since both the spatial extent to which H_A penetrates into the superconductor and its derivative at the surface are determined by the same length. Because of the tensorial nature of the penetration depth, once the principal values are determined, the results of any experiment involving applying $\mathbf{H}_\mathrm{A}$ along an arbitrary angle ψ with respect to e.g., the a axis can be elucidated, although the result will depend on the specific experiment considered.

In the presence of nonlinear effects, the situation is much more complicated. Because of the nonlinearities, the superfluid density or the penetration length are no longer tensors. Also[31,37] the lengths that characterize the surface derivatives and the extent of field penetration differ by significant numerical factors. Several possible definitions of the effective $\lambda(\psi)$ which coincide in the linear limit give different results for $\lambda(\psi, H_A)$ in the nonlinear case. In general, experimentally one measures the extent to which fields penetrate and definitions involving surface derivatives are not appropriate. To find the right definition one must consider the experimental setup. In the experiments of Ref. 36, the crystal is rotated to different orientations with respect to the field and a measurement of the component of the magnetic moment $\mathbf{m}$ along the applied field is performed. The penetration depth $\lambda(\psi)$ is then extracted[40,41] through the relation:

$$m^{\|}(\psi) = -\frac{H_A V}{4\pi}\left(1 - \frac{2\lambda(\psi)}{d}\right) \tag{2.1}$$

where $m^{\|}$ is the component of $\mathbf{m}$ along the field and V the volume of the sample. The term in 2.1 involving the effective penetration depth depends only on the sample area A in the direction parallel to the field. One can equivalently write this definition of $\lambda(\psi, H_A)$ in terms of the integral of the appropriate component of the field by making use of standard identities.[34,42,43] One then has

$$\lambda(\psi, H_A) = \int_0^{d/2} dz\, H^{\|}(\psi, H_A, z)/H(0), \tag{2.2}$$

where $H^{\|}$ is the component of $\mathbf{H}(z)$ parallel to the applied field. This is the definition of $\lambda(\psi)$ we will use. Other definitions may have to be employed for different experimental setups. However, once the nonlinear field distributions inside the sample are known it is a rather easy matter, as seen below, to extract the effective λ corresponding to any other alternative definition.

To separate the nonlinear effects we write:

$$\lambda(\psi, H_A) = \lambda_{lin}(\psi) + \Delta\lambda(\psi, H_A) \tag{2.3}$$

Since the linear part is field independent while the nonlinear part, as we shall see below, vanishes at zero field, one has that the nonlinear part $\Delta\lambda(\psi, H_A) = \lambda(\psi, H_A) - \lambda(\psi, H_A = 0)$. We will see that λ_{lin} has the expected angular behavior. The nonlinear part can be written in terms of the nonlinear magnetic moment m_{nl} as:

$$\Delta\lambda(\psi, H_A) = \frac{2\pi}{H_A A} m_{nl}^{\|}(\psi, H_A), \tag{2.4}$$

where $m_{nl}^{\|}$ is the parallel component of m_{nl}. Since m_{nl} is an extensive quantity, proportional to the sample area, we see from (2.4) that $\Delta\lambda$ is intensive. Using the expression for the magnetic moment in terms of the current field $\mathbf{j}$, $\mathbf{m} = \frac{1}{2c}\int \mathbf{dr}(\mathbf{r}\times\mathbf{j})$, standard identities[42,43] and the London and Maxwell equations, (2.4) can be expressed entirely[34] in terms of the value of the nonlinear flow field $\mathbf{v}$ at the surface of the sample. This will be done explicitly for several cases. We first however, give a brief outline below on the procedure for calculating the nonlinear fields in the cases where they are not yet known.

B. Calculation of the fields

In some of the cases of interest we will be able to use the field distributions found in previous work[34], but in several others the fields must be calculated. We explain here briefly the method involved, with details of the calculations in the Appendices.

Within the framework[28] of the nonlinear Meissner effect, the relation[31] between $\mathbf{j}$ and $\mathbf{v}$ is a sum or linear and nonlinear parts, $\mathbf{j}(\mathbf{v}) = \mathbf{j}_{lin}(\mathbf{v}) + \mathbf{j}_{nl}(\mathbf{v})$, where $\mathbf{v}$ is the flow field, and $\mathbf{j}$ is the supercurrent. The linear part is the usual relation $\mathbf{j}_{lin} = -e\tilde{\rho}\mathbf{v}$, where $\tilde{\rho}$ is the superfluid density tensor, while the nonlinear term[30,31] in the low temperature limit considered here is:

$$\mathbf{j}_{nl}(\mathbf{v}) = -2eN_f^* \int_{FS} d^2s\, n(s)\mathbf{v}_f \sqrt{(\mathbf{v}_f\cdot\mathbf{v})^2 - |\Delta(s)|^2}\,\Theta(-\mathbf{v}_f\cdot\mathbf{v} - |\Delta(s)|). \tag{2.5}$$

Here N_f^* is the total density of states at the Fermi level, and $n(s)$ is the local density of states at the point s on the Fermi surface (FS), normalized to unity. The step function in (2.5) restricts the integration over the FS by

$$|\Delta(s)| + \mathbf{v}_f\cdot\mathbf{v} < 0. \tag{2.6}$$

The functional relationship between $\mathbf{j}$ and $\mathbf{v}$ is then combined with the Maxwell-London equation,[28,29]

$$\nabla\times\nabla\times\mathbf{v} = \frac{4\pi e}{c^2}\mathbf{j}(\mathbf{v}). \tag{2.7}$$

Using the boundary conditions, $\nabla\times\mathbf{v}|_{d/2} = (e/c)\mathbf{H}_{\mathrm{A}}$, and $\mathbf{v}(0) = 0$, we can, for the geometry under consideration, solve (2.7) analytically for the necessary fields and then extract $\Delta\lambda$ from (2.4).

III. RESULTS

It is convenient to introduce several dimensionless quantities used in the calculations. These are the dimensionless coordinate ζ_i which represents the coordinate perpendicular to the plane surface of the sample (measured from its midpoint) in units of λ_i, the appropriate penetration depth tensor component in the sample plane. Its surface value is $\zeta_{s,i} \equiv d/(2\lambda_i)$. The dimensionless nonlinear flow field,

$$u_{nl,i} \equiv \frac{v_{nl,i}}{\tilde{v}}, \tag{3.1}$$

is normalized by the characteristic linear velocity,

$$\tilde{v} \equiv \frac{e}{c}\lambda H_A, \tag{3.2}$$

where λ is defined in each case from the in-plane components of the linear penetration depth.

A. 2-D nodal lines with YBCO type othorhombicity

As our first example, we examine the nonlinear effects associated with a two-dimensional gap that has nodal lines, with crystal orthorhombicity of the YBCO type,[34,44] that is, with the nonequivalent a and b axes being along the antinodal directions. The applied field is in the $a-b$ plane, forming an angle ψ with the a axis, so that the fields have a and b components, which depend only on the coordinate z. Considering the usual linear term only, it is completely elementary to verify that the definition (2.1) yields $\lambda_{lin} = \lambda_b \cos^2\psi + \lambda_a \sin^2\psi$, independent of the magnitude H_A. We can turn then to the nonlinear $\Delta\lambda$.

The four line nodes are symmetrically placed at angles φ_n (measured from the positive a-axis), where $n = 1,...,4$ labels the node. The Fermi velocity at φ_1 forms an angle α with the $+a$ axis. These angles are shown in Fig. 1. In the presence of orthorhombic distortion, φ_1 need not equal $\pi/4$, and α does not have to be equal to φ_1. One often characterizes the deviation of φ_1 from $\pi/4$ by describing the order parameter as being "$d+s$" writing for example $\Delta(\varphi) = \Delta_d \cos(2\varphi) + \Delta_s$, and then introducing a separate angular variable (see Ref. 34), for the orientation of the Fermi velocity. This may be misleading, however, since it is in this case no longer accurate to classify the OP in terms of angular momentum waves. More important, since the nonlinear results depend only on the *local* properties at the nodal positions, there is *only one* relevant angular variable, which is α, regardless[45] of which origin one wishes to ascribe to it.[46]

We can see from the Fig. 1 that the magnitude of $\mathbf{v}_f$ is the same at all nodes, and that we can restrict the angle $\mathbf{H}_\mathrm{A}$ makes with the a axis to $\psi \in [0, \pi/2]$. We characterize the anisotropy of the linear penetration depth tensor by $\Lambda_a \equiv \lambda_a/\lambda_b$, and it suffices to take $\Lambda_a \geq 1$. Only the local properties of the OP near the nodes contribute to the nonlinear current, hence we express the OP near the nodes as,

$$\Delta(\varphi) \approx 2\Delta_0(\varphi - \varphi_n), \tag{3.3}$$

where Δ_0 is half of the slope of the OP near the nodes, and should not necessarily be identified with the gap maximum.

When $\psi \in [0, \pi/2]$, we have (see 2.6) the possibility of quasiparticle activation (QPA) at the nodes labeled (see Fig. 1) (1) and (2), *or* at (2) and (3). The specific nodal pair that is activated depends on which nodal $\mathbf{v}_f$ satisfy the restriction in (2.6). Anisotropy in the penetration depth tensor leads to $\mathbf{v}$ twisting (with increased depth from the surface) towards the axis with the larger penetration depth, which is a. This effect occurs at linear order and it is therefore very significant. The nodes which contribute to the nonlinear term, therefore, depend on the dimensionless coordinate $\zeta_i \equiv z/\lambda_i$ within the sample. There are three cases to consider: The first is when $\psi \in [0, \psi_1]$, where ψ_1 is the maximum ψ that will result in QPA solely at (1) and (2). This angle is very small except when $\Lambda_a \gtrsim 1$. The second case is when $\psi \in [\psi_1, \psi_2]$, where ψ_2 is the maximum ψ that will give QPA at nodes (1) and (2) until a depth ζ_a^* is reached, then there is a crossover, and subsequent QPA at nodes (2) and (3). The third region has $\psi \in [\psi_2, \pi/2]$, where the only nodes activated at any depth are at (2) and (3).

The nonlinear current-flow relation for the case when there is QPA at nodes (1) and (2) is calculated by inserting the OP, Eq. (3.3) into (2.5). The main steps are carried out in Appendix A. We find in Eq. (A3a) for the a-component,

$$j_{nl,a} = -2\, e\rho \frac{v_a v_b}{v_c} \cos^2\alpha \sin\alpha. \tag{3.4}$$

Here $\rho \equiv \frac{1}{2} N_f v_f^2$, is the local value of the superfluid density at the nodes, N_f is the local density of states, v_f is the Fermi speed at the nodes, and the local critical velocity is $v_c \equiv \Delta_0 / v_f$. Similarly, when there is QPA at (2) and (3), the a-component of the current is given by (A4a),

$$j_{nl,a} = \frac{e\rho}{v_c} \cos\alpha \left[v_a^2 \cos^2\alpha + v_b^2 \sin^2\alpha \right]. \tag{3.5}$$

Analogous expressions can be written for the b-component. To find the nonlinear flow field we insert the current (3.4) into (2.7), for $\zeta_a \in [\zeta_a^*, \zeta_{s,a}]$ or (3.5) for $\zeta_a \in [0, \zeta_a^*]$. The solution is found perturbatively (to first order) using the previously stated boundary conditions plus continuity of the flow field, magnetic field, and current at the crossover point ζ_a^*. The details are given in Appendix B, the main results are (B4) and (B10). We choose $\lambda \equiv \sqrt{\lambda_a \lambda_b}$ as the normalization in (3.2), and we take[34] $\lambda = \lambda_n$, its nodal value. H_0 is the usual[31,34] characteristic field,

$$H_0 = \frac{c\Delta_0}{e\lambda v_f}. \tag{3.6}$$

We can now achieve our objective, and get $\Delta\lambda$ from the calculated fields. We write (2.4) in terms of the dimensionless flow field,

$$\Delta\lambda = \lambda \left[\sin\psi \, u_{nl,a}(\zeta_{s,a}) - \cos\psi \, u_{nl,b}(\zeta_{s,b}) \right]. \tag{3.7}$$

The flow field results in Appendix B are valid for any material thickness d. Upon taking the slab limit $d \gg \lambda$, we can express $\Delta\lambda(\psi)$ in the following form:

$$\Delta\lambda(\psi, H_A) = \frac{1}{6} \frac{H_A}{H_0} \lambda \mathcal{Y}(\psi). \tag{3.8}$$

We see from this result that the nonlinear effect in the penetration depth is proportional to the field, for line nodes. The quantity $\mathcal{Y}(\psi)$ represents its angular dependence, normalized so that its maximum is unity for the tetragonal case. The function $\mathcal{Y}$ has a different expression for each region of ψ, with the crossover angles ψ_1, ψ_2 being given in (B1). These expressions are:

$$\mathcal{Y}(\psi) = \frac{18\Lambda_a}{2+\Lambda_a} \cos^2\alpha \sin\alpha \sin^2\psi \cos\psi + \frac{2}{\Lambda_a^2} \sin^3\alpha \cos^3\psi, \qquad \psi \in [0, \psi_1], \tag{3.9a}$$

$$\begin{aligned} \mathcal{Y}(\psi) = {} & \frac{18\Lambda_a}{2+\Lambda_a} \cos^2\alpha \sin\alpha \cos\psi \sin^2\psi \\ & + \frac{2}{\Lambda_a^2(1+2\Lambda_a)} \sin^3\alpha \cos^3\psi \Big[1 + 2\Lambda_a + (4\Lambda_a - 1) \left(\frac{\Lambda_a \tan\psi}{\tan\alpha} \right)^{\frac{3\Lambda_a}{\Lambda_a - 1}} \Big] \\ & + \frac{2\Lambda_a^2(2\Lambda_a^2 - 10\Lambda_a - 1)}{(2+\Lambda_a)(1+2\Lambda_a)} \cos^3\alpha \sin^3\psi \left(\frac{\Lambda_a \tan\psi}{\tan\alpha} \right)^{\frac{3}{\Lambda_a - 1}}, \qquad \psi \in [\psi_1, \psi_2], \end{aligned} \tag{3.9b}$$

$$\mathcal{Y}(\psi) = \frac{18}{1+2\Lambda_a} \sin^2\alpha \cos\alpha \cos^2\psi \sin\psi + 2\Lambda_a^2 \cos^3\alpha \sin^3\psi, \qquad \psi \in [\psi_2, \frac{\pi}{2}]. \tag{3.9c}$$

When $\Lambda_a = 1$, $\psi_1 = \psi_2 = \alpha$ and the middle one of the expressions above is not needed. We present plots for $\mathcal{Y}(\psi)$ in the next three Figures, where ψ is limited to $0 < \psi < \pi/2$, since the result in the remaining range is trivially obtained by symmetry. In Fig. 2, we show results for fixed $\alpha = \pi/4$, and vary the anisotropy parameter Λ_a of the penetration depth tensor, which influences the result through the twisting of the fields inside the sample. For reference, we plot the isotropic result as the bold curve. The ratio of $\sqrt{2}/2$ between the minima and maxima of this reference curve has been known for a long time.[28] We consider the range $1.0 - 1.5$ for Λ_a, in increments of 0.1. We see that as this parameter increases, the symmetry of the curve changes, to reflect the mixing of $\pi/2$ and π symmetries. The signal increase with Λ_a when $\psi = \pi/2$, can readily be understood physically, since the volume occupied by the currents will be in this case determined by the larger of the linear components. We can see from the Figure the signal characteristics change considerably with increasing anisotropy. The maxima and minima of $\mathcal{Y}$ are no longer separated by the factor of $\sqrt{2}/2$ for $\Lambda_a > 1.0$. With sufficiently large Λ_a, as seen in the Figure, the signal at $\psi = \pi/4$ becomes approximately the average of $\mathcal{Y}(\psi = 0)$ and $\mathcal{Y}(\psi = \pi/2)$. This illustrates the high sensitivity of the penetration depth to anisotropy, as compared with the previously studied[34] transverse magnetic moment. The reason for this difference in the transverse and longitudinal behaviors is explained in the last Section.

Next, in Figure 3, we examine the effects of varying α while keeping $\Lambda_a = 1.0$ fixed. Again, the bold curve is the $\alpha = \pi/4$ result, and the other curves are for values $\alpha = (\pi/4) \pm n\delta\alpha$ with $n = 1, 2, 3$ and $\delta\alpha = \pi/80$. It is seen that, at $\psi = 0$, the signal increases as α increases above $\pi/4$, reflecting the increase in $|\mathbf{v} \cdot \mathbf{v}_f|$. For smaller values of α the effect reverses, with the curves corresponding to the same n and opposite sign being symmetric with respect to exchange of the a and b axes. This behavior is very sensitive to small changes in α. The effects of increasing α are in a sense opposite to those of increasing Λ_a. It is interesting therefore to see how these two effects combine. Thus, in Fig. 4, we plot the normalized $\Delta\lambda$ for $\Lambda_a = 1.3$, and the same values of α as in Fig. 3. The symmetry of the curves for the same n is now lost, because $\Lambda_a \neq 1$. The overall conclusion that one can draw from these results is that in the presence of even relatively moderate deviations from the tetragonal "pure d-wave" situation, the appearance of the $\Delta\lambda(\psi)$ vs ψ data might reflect more a π than a $\pi/2$ symmetry. This has to be kept present in analyzing experimental results. We will return to this point in Section IV.

B. 2-D line nodes/orthorhombicity of BSCCO type

Next we consider the nonlinear effects associated with a two-dimensional OP with line nodes in the presence of orthorhombic anisotropy characteristic of $Bi_2Sr_2CaCu_2O_{8+\delta}$ (BSCCO) materials. The new orthorhombic a and b axes of symmetry form angles of $\pi/4$ with the undistorted tetragonal axes. In this case, the nodes are at angles of $\pi/2$ from each other and the nodal Fermi velocities are aligned with the nodal directions, which are the principal axes of the system. However, the two nodes on the new a axis are not equivalent to the other two on the new b axis. The fields for this case were calculated in Section IIIA.2 of Ref. 34. We need only to insert these fields into (3.7) and get (for $d \gg \lambda_i$),

$$\Delta\lambda(\psi, H_A) = \frac{1}{6}\frac{H_A}{H_0}\lambda\mathcal{B}(\psi), \tag{3.10}$$

where $\lambda \equiv \sqrt{\lambda_{na}\lambda_{nb}}$, with $\lambda_{ni} \equiv (2\pi e^2/c^2)N_f v_{fni}^2$, where v_{fni} are the nodal Fermi velocities, H_0 is defined in (3.6) with $v_f = \sqrt{v_{fna}v_{fnb}}$, and we take $\lambda_{ni} = \sqrt{\lambda_a\lambda_b}$. Here the simple angular dependence is contained in the factor $\mathcal{B}(\psi)$, and is given by

$$\mathcal{B}(\psi) = \Lambda_a^{-1/2}\cos^3\psi + \Lambda_a^{1/2}\sin^3\psi. \tag{3.11}$$

In Fig. 5, we show $\mathcal{B}(\psi)$ for varying degrees of anisotropy, $\Lambda_a = 1.0 - 1.5$ in increments of 1/10.

C. 2-D quasinodal lines

Now we turn to the situation where there are no nodes, but rather, very deep minima in the gap function (quasinodes). This can be due to a small, constant $i\Delta_s$ or $i\Delta_{d_{xy}}$ component in the OP, which we assume is added to a main $\Delta_{d_{x^2-y^2}}$ component. The OP near the quasinodes can then be written in the form

$$\Delta(\varphi) = i\Delta_{\min} + 2\Delta_0(\varphi - \varphi_n), \tag{3.12}$$

where $2\Delta_0$ is the slope of the OP at the minima of the gap function, and $\Delta_{\min} \ll \Delta_0$ is the minimum value of the energy gap. Here we consider only the isotropic case $\lambda_a = \lambda_b \equiv \lambda$, $\alpha = \pi/4$, which is sufficient to illustrate the changes brought about by the presence of quasinodes, rather than nodes, and where we can use previously calculated field distributions from Section IV of Ref. 34. We insert these fields into (2.1). The resulting nonlinear $\Delta\lambda$ depends on two variables, besides the angle ψ: the ratio $h \equiv H_A/H_0$ of the applied field to the characteristic field H_0, defined in (3.6), and the ratio

$$\kappa \equiv \frac{\Delta_{\min}}{\Delta_0}\bigg/\frac{H_A}{H_0}. \tag{3.13}$$

We find after straightforward algebra, in the $d \gg \lambda$ limit,

$$\Delta\lambda(\psi, H_A) = \frac{1}{6}\lambda\frac{H_A}{H_0}\mathcal{Q}(\psi, \kappa). \tag{3.14}$$

The angular and field dependences now no longer factorize and are (apart from the overall factor of h) represented by the function of two variables $\mathcal{Q}$, which is normalized to unity at $\psi = 0$, $h = 0$:

$$\mathcal{Q}(\psi,\kappa) = (\cos\psi' - \kappa)^2(2\kappa + \cos\psi')\Theta\left(\cos\psi' - \kappa\right) + (\sin\psi' - \kappa)^2(2\kappa + \sin\psi')\Theta\left(\sin\psi' - \kappa\right), \tag{3.15}$$

written for $0 \leq \psi' \leq \pi/2$ (trivially extended by symmetry to the remaining range) with $\psi' \equiv \psi - \pi/4$. The step functions imply that the nonlinear effects vanish for $h < \delta$, with $\delta \equiv \Delta_{\min}/\Delta_0$, since then the field is not sufficiently strong to create quasiparticles of energy larger than the minimum gap value. The behavior of $\mathcal{Q}(\psi,\kappa)$ is plotted in Fig. 6, where we show its angular dependence for several values of κ, with the applied field above threshold. One can see how the filling of the node produces a fast decrease in the nonlinear effect on the penetration depth, as it does[35] also for the transverse moment. In Fig. 7, the variation of $\Delta\lambda/\lambda$ as a function of H_A/H_0 is shown for several values of δ, at $\psi = \pi/4$. The field threshold effect is clearly seen, and can be read off directly from the curves.

D. 3-D quasinodal points and lines

We now examine cases where the FS is three-dimensional and the nodal or quasinodal structure of the energy gap involves points or lines. We will consider here the same situation for which, in the limit of pure nodes, the transverse magnetic moment was calculated in Ref. 37. For the sake of brevity, we will compute directly the fields in the quasinodal case, and consider the situation where actual nodes exist as the appropriate special limit. For both of the cases considered below, we will assume that the slab surfaces are parallel to the $a-c$ plane, and that $\mathbf{H}_{\mathrm{A}}$ is also in this plane, with ψ defined with respect to the c axis. Then, the nonlinear fields have only x or z components (depending on whether we are discussing lines or point nodes respectively, see below), which depend only on the coordinate y normal to the sample. Again it is elementary to show that $\lambda(\psi,H_A) = \lambda_{lin}(\psi) + \Delta\lambda(\psi,H_A)$, where $\lambda_{lin}(\psi) = \lambda_z \sin^2\psi + \lambda_x\cos^2\psi$, independent of H_A and

$$\Delta\lambda(\psi,H_A) = \lambda_z \sin\psi\, u_{nl,z}(\zeta_{s,z}) - \lambda_x\cos\psi\, u_{nl,x}(\zeta_{s,x}). \tag{3.16}$$

We will use this result with the fields calculated below.

1. 3-D point nodes

We first consider an OP leading to a gap with two quasinodes at the poles along the z-axis. In this configuration, the nonlinear fields have only a z-component, which depends on the coordinate y. By symmetry, we can restrict our analysis to the quasinode at $\theta = 0$, where θ is the usual polar angle. We take the form of the gap near the quasinode to be

$$|\Delta(\theta)| = (|\Delta_{\min}|^2 + |\Delta_p\theta|^2)^{1/2}, \qquad \theta \approx 0, \tag{3.17}$$

where Δ_p is the slope of the OP near the node, and $\delta \equiv \Delta_{\min}/\Delta_p \ll 1$. This is the generalization of the previously studied[37] OP to the quasinodal case.

The nonlinear current response as a function of the flow field is calculated in Appendix A, and we find, for its only nonzero component,

$$j_{nl,z} = \frac{e\rho}{v_p^2}\left(v_z^2 - v_s^2\right)^{3/2}\Theta(v_z - v_s), \tag{3.18}$$

where $v_p \equiv \Delta_p/v_f$, $v_s \equiv \Delta_{\min}/v_f$, and in three dimensions, $\rho \equiv \frac{1}{3}N_f v_f^2$ in terms of local values. This result shows that there are no nonlinear effects present if $v_z < v_s$. Since the flow field decreases with distance into the sample, there will be a depth in the material, which, in terms of the dimensionless variable $\zeta_z \equiv y/\lambda_z$, we denote as ζ_z^*, where $v_z = v_s$, so that nonlinear corrections are absent for the region below ζ_z^*. Inserting (3.18) into (2.7), we get an equation for the flow field. This equation can be solved perturbatively to first order in the small parameter $(H_A/H_0)^2$, where $H_0 \equiv c\Delta_p/e\lambda_z v_f$. In Appendix B we find, taking into account these subtleties, the solution $u_{nl,z}(\zeta_z)$ for arbitrary thickness d. The result is given in (B14). We then have from (3.16) and (B14), after taking the limit $d \gg \lambda_z$, the result, valid for $0 < \psi < \pi/2$,

$$\Delta\lambda(\psi,H_A) = \frac{1}{4}\lambda_z\frac{H_A^2}{H_0^2}\mathcal{P}(\psi,\kappa)\Theta(\sin\psi - \kappa), \tag{3.19}$$

where the function $\mathcal{P}(\psi,\kappa)$ is given by,

$$\mathcal{P}(\psi,\kappa) = \frac{3}{2}\kappa^4 \ln\left(\frac{\sin\psi + \sqrt{\sin^2\psi - \kappa^2}}{\kappa}\right) + \left(\sin^3\psi - \frac{5}{2}\kappa^2 \sin\psi\right)\sqrt{\sin^2\psi - \kappa^2}. \tag{3.20}$$

Here we see the mixed angular and field dependence of the result, as in the function $\mathcal{Q}$ in (3.15). The step function parameter, involving the quantity

$$\kappa \equiv \frac{\Delta_{\min}}{\Delta_p} \bigg/ \frac{H_A}{H_0}, \tag{3.21}$$

reflects again the requirement that the appropriate field component exceed a minimum value. In Fig. 8, we plot $\mathcal{P}(\psi,\kappa)$, for various values of κ with the applied field above threshold. One again can see the decrease of the effect as the minimum gap value increases. The inset contains the field dependence of $\Delta\lambda/\lambda_z$ at $\psi = \pi/2$, for $\delta = 0 - 0.04$, in increments of 0.01. There we can see that the field dependence above threshold is no longer parabolic, as is the case when $\Delta_{\min} = 0$.

2. 3-D line nodes

Finally, we consider a three dimensional FS with a quasinodal line in the $x-y$ plane. The angular dependence of the gap near the quasinodal line at $\theta = \pi/2$ has the form,

$$|\Delta(\theta)| = (|\Delta_{\min}|^2 + |\Delta_p(\frac{\pi}{2} - \theta)|^2)^{1/2}, \qquad \theta \approx \frac{\pi}{2}, \tag{3.22}$$

with $\Delta_{\min} \ll \Delta_p$. The transverse magnetic moment in the $\Delta_{\min} = 0$ limit of this OP has been previously[37] studied. For this case, the fields only have x components, and we assume tetragonal symmetry. We calculate the nonlinear current in Appendix A where we find,

$$j_{nl,x} = \frac{e\rho}{v_p v_x}\left(v_x^2 - v_s^2\right)^{3/2} \Theta(v_x - v_s). \tag{3.23}$$

Again, the nonlinear current vanishes unless the flow field, v, is sufficiently large; $v_x > v_s$. Once (3.23) is inserted into (2.7), we get an equation for the flow field that can be solved with a procedure identical to the point node case. This is done in Appendix B. We find in the thick slab limit, for the only nonzero component:

$$u_{nl,x}(\zeta) = \frac{H_A}{H_0}\left[E_1 e^{\zeta} + E_2 e^{-\zeta} + r(\zeta)e^{\zeta} + s(\zeta)e^{-\zeta}\right], \tag{3.24}$$

where $H_0 \equiv c\Delta_p/e\lambda v_f$, $\zeta \equiv y/\lambda$, λ is the linear penetration depth in the $a-b$ plane, and the constants E_1, E_2, and the functions r, and s are given in Appendix B. The nonlinear correction to the penetration depth is then obtained from (3.16) and (3.24), as:

$$\Delta\lambda = \frac{1}{3}\lambda\frac{H_A}{H_0}\mathcal{L}(\psi,\kappa)\Theta(\cos\psi - \kappa), \tag{3.25}$$

where $\mathcal{L}(\psi,\kappa)$ is normalized so that its maximum at $\kappa = 0$ is unity,

$$\mathcal{L}(\psi,\kappa) = 3\kappa^3 \tan^{-1}\left(\frac{\sqrt{\cos^2\psi - \kappa^2}}{\kappa}\right) + \left(\cos^2\psi - 4\kappa^2\right)\sqrt{\cos^2\psi - \kappa^2}. \tag{3.26}$$

The overall power law behavior at $\Delta_{\min} = 0$ is now linear in the field, and at finite $\Delta_{\min}$ a threshold effect is found. We plot these results in Fig. 9, where we display $\mathcal{L}(\psi,\kappa)$, for various values of κ. The resulting behavior is very reminiscent from that found in the previous case. The inset contains the field dependence of $\Delta\lambda/\lambda$ at $\psi = 0$, with δ having the same values as in Fig. 8. Because of the mixed dependence of these results on the field and angular variables, the curves shown are not linear, except in the case $\delta = 0$, and again the threshold values can be read off directly from the intercepts.

IV. DISCUSSION AND CONCLUSIONS

In summary, prompted by recent refinements in experimental techniques that allow very high precision measurements of $\Delta\lambda$, and by the ever increasing number of candidates for unconventional superconducting states, we have calculated the low temperature angular and field dependence of the nonlinear component to the penetration depth for several different two and three dimensional energy gaps with nodal or quasinodal structures.

The expected signal for the nonlinear penetration depth effect exceeds the available experimental resolution[36,47] of one tenth of an Ångstrom by a considerable factor. To see this, consider for example a tetragonal compound with pure d-wave pairing and a linear penetration depth $\lambda = 1400$Å, in the YBCO range. From (3.8), we easily get that the difference $\delta\lambda \equiv \Delta\lambda_{\max} - \Delta\lambda_{\min}$, between the minimum and maximum values of $\lambda(\psi)$ would be, at $h = 0.04$, about 3 Å, a factor of thirty better than the experimental resolution. This is an order of magnitude improvement when compared to the corresponding estimate, under the same assumptions, for measurements of the the transverse magnetic moment where one has at best[35] a factor of three. Further, taking into account the orthorhombicity of YBCO by setting[48] $\Lambda_a = 1.6$, which increases $\delta\lambda$ (see Fig. 2), we find from the same equation and at the same h, $\delta\lambda \approx 14$Å. This is a factor of 140 above the resolution achieved in Refs. 36,47.

For gap functions with line nodes, we have found that $\Delta\lambda$ at fixed angle is proportional to the field. Our results, however, are obtained in the low temperature, clean limit. Both finite temperature[30] and impurities[30,29] modify this linear behavior at smaller fields, where nonlocal effects[49] may have a similar influence.[50] Since the combined outcome of these effects is not at present amenable to reliable computation, it is safer to perform the experiments and to compare with theory at the largest possible fields, where the behavior should approach linearity. H_A can be increased all the way to the field of first flux penetration, H_{f1}, taking in this full advantage of this field being in practice[35,50] much larger than the Ginzburg-Landau estimate of H_{c1}.

Keeping this in mind, let us consider our results for two-dimensional gap functions with nodes for materials with YBCO-type orthorhombicity. Some experimental results for the angular dependence of $\lambda(\psi)$ for YBCO are available,[36] although only for a few selected directions. We have found that the angular dependence of $\lambda(\psi)$ is extremely sensitive (see Fig. 2) to small departures from unity in the anisotropy factor Λ_a, eventually resulting in a change in the apparent leading symmetry behavior of $\Delta\lambda(\psi)$, which then looks quite different from that found in the tetragonal case. Taking again $\Lambda_a = 1.6$, for[48] YBCO, we find that $\mathcal{Y}(\psi = 0) \approx 0.30$, $\mathcal{Y}(\psi = \pi/2) \approx 1.8$, while $\mathcal{Y}(\psi = \pi/4) \approx 1.2$, very close to the average in the two main axial directions. This is precisely what it is found experimentally.[36] Because this is so different from what happens when $\lambda_a = \lambda_b$, it was mistakenly interpreted in the experimental work as evidence against, instead of for, the anisotropy found there being due to the nonlinear Meissner effect. The measured field dependence[36] departs considerably at small fields from linearity. This is apparently[36,40] not due to temperature effects alone and we believe it is very likely attributable to impurities, since the zero field temperature dependence of λ of the sample used departs appreciably from linearity for temperatures below about 3 K. At the largest fields, the field dependence extrapolates to linear, with reasonable values of $H_0 \approx 9000$ gauss. Thus, these experimental results are consistent, as far as their field and angular dependence, with our theory. The weak temperature dependence of these and other[47] measurements remains, however, a puzzle. It cannot be ruled out, given the complications involving the correct treatment of impurity averaging[51] in these materials, that the temperature has a relatively weak effect in the samples studied. Further experimental work in the same or other materials is needed. Preliminary results for single crystals of TI-2201 show $\Delta\lambda$ having a linear magnetic field dependence that is interpreted[52] as agreeing with theoretical expectations for the nonlinear Meissner effect.

This strong sensitivity of $\Delta\lambda$ to anisotropy (either to Λ_a or to α, the angle that $\mathbf{v}_f$, at the node, makes with the $+a$ axis) would not be expected from previous calculations[34] of the transverse magnetic moment, where the effects of orthorhombicity were not pronounced. The reason is that the transverse moment is constrained by symmetry to vanish, regardless of orthorhombicity, both at $\psi = 0$ and at $\psi = \pi/2$, plus at one point in between. This constraint does not exist for a longitudinal measurement.

We have also examined gaps with two-dimensional quasinodes, and found that the field and angular dependence are no longer separable. The angular and field dependence of $\Delta\lambda$ is governed by a term linear in the field and by a step function indicating that a minimum threshold field must be applied to excite quasiparticles above the gap minimum. This is multiplied by a function of ψ and of the parameter κ, which is a ratio (see (3.13)) relating the value of the gap minimum to the applied field strength. The signal decreases markedly as κ increases.

In Subsection III D, we investigated three dimensional gaps with points and line quasinodes. There again the nonlinear contribution to the penetration depth depends on a function of angle and of a parameter κ now defined in (3.21), a step function, and a separate factor linear in the applied field for line nodes and quadratic for points. The situation is similar, as far as the field dependence, to that for the two-dimensional case. The signal decreases with increasing κ and vanishes at threshold. For example, at $\kappa = 0.6$, the nonlinear signals for both points and lines drop to about 25% of their maximum ($\kappa = 0$) values. Even with such large admixtures, however, the signal is still likely to be within current experimental resolution. Let us estimate the signal for an OP with three dimensional line nodes, similar to that which might occur in Sr_2RuO_4, or certain[9] heavy fermion compounds. Using (3.25), with $\kappa = 0$, we find, $\delta\lambda = \Delta\lambda_{\max} = \frac{1}{3}\lambda h$. Using published[19] values for Sr_2RuO_4 we estimate $\lambda = 2000$Å and a value $h = 0.3$ for $H_A = H_{c1}$. These values give a maximum signal of, $\delta\lambda \approx 200$Å. The magnitude of the signal in this case is well above experimental resolution, and even with relatively large admixture leading to a substantial $\Delta_{\min}$ the signal would still be experimentally tangible.

We have focused here on the nonlinear effects on the angular dependence of the penetration depth, and we have shown the strong influence that anisotropy in the principal values of the linear penetration depth and orientation of the Fermi velocity has on the results. The methods presented in this paper can be readily extended to other nodal patterns and to include the nonlinearities in the temporal response that arise from a time-dependent magnetic field.[53,54] These phenomena are currently being investigated via microwave measurements.[55]

ACKNOWLEDGMENTS

We thank A. Bhattacharya for many conversations, C. Bidinosti for providing us with much information about his experimental methods and S.M. Anlage for insightful discussions with I.Ž. This work was supported in part by the Petroleum Research Fund, administered by the ACS (at Minnesota) and by the US ONR Grant N000140010028 and DARPA (at Maryland).

APPENDIX A: CURRENTS

1. 2-D nodal lines with orthorhombicity

For the order parameter given by (3.3), the four line nodes are symmetrically placed (see Fig. 1) at angles φ_n, measured from the positive a-axis, where $n = 1,...,4$ labels the node. The Fermi velocity at node 1 is $\mathbf{v}_f^{(1)} = v_f(\cos\alpha, \sin\alpha)$. After making the replacement $N_f^* \int_{FS} d^2s\, n(s) \to N_f \int_{\bar{\varphi}_c} d\varphi/2\pi$, Eq. (2.5) gives the contribution, $\mathbf{j}_{nl}^{(n)}$, when quasiparticles at φ_n are activated:

$$\mathbf{j}_{nl}^{(n)}(\mathbf{v}) = -2eN_f \int_{-\bar{\varphi}_c}^{\bar{\varphi}_c} \frac{d\bar{\varphi}}{2\pi}\, \mathbf{v}_f \sqrt{(2\Delta_0\bar{\varphi}_c)^2 - (2\Delta_0\bar{\varphi})^2}, \tag{A1}$$

where $\bar{\varphi} \equiv \varphi - \varphi_n$, and the integration is limited by $\bar{\varphi}_c = |\mathbf{v}_f \cdot \mathbf{v}|/(2\Delta_0)$. One finds,

$$\mathbf{j}_{nl}^{(n)} = -\frac{e}{4\Delta_0} N_f \mathbf{v}_f^{(n)} [\mathbf{v}_f^{(n)} \cdot \mathbf{v}]^2. \tag{A2}$$

Except when $\mathbf{v}$ is along a nodal Fermi velocity, in general two nodes must be considered. If the nodes at φ_1 and φ_2 are activated, we can get the total nonlinear current by adding $\mathbf{j}_{nl}^{(1)} + \mathbf{j}_{nl}^{(2)}$ from (A2):

$$j_{nl,a} = -2\, e\rho \frac{v_a v_b}{v_c} \cos^2\alpha \sin\alpha, \tag{A3a}$$

$$j_{nl,b} = -\frac{e\rho}{v_c} \sin\alpha \left[v_a^2 \cos^2\alpha + v_b^2 \sin^2\alpha\right]. \tag{A3b}$$

where we have introduced the local superfluid density, $\rho \equiv (1/2) N_f v_f^2$, and critical velocity $v_c = \Delta_0/v_f$. Likewise, if the nodes at φ_2 and φ_3 are activated, we get

$$j_{nl,a} = \frac{e\rho}{v_c} \cos\alpha \left[v_a^2 \cos^2\alpha + v_b^2 \sin^2\alpha\right], \tag{A4a}$$

$$j_{nl,b} = 2\, e\rho \frac{v_a v_b}{v_c} \sin^2\alpha \cos\alpha. \tag{A4b}$$

2. Nonlinear current for 3-D quasinodes

a. 3-D point quasinodes

We examine first a gap of the form (3.17). By symmetry, we can restrict ourselves to the node at $\theta = 0$ since the contribution from $\theta = \pi$ is identical. Thus, $\mathbf{v}_f \approx (0, 0, v_{fz})$, and the relevant region of integration is limited by θ_c, as determined from $(\mathbf{v}_f \cdot \mathbf{v})^2 = |\Delta(\theta_c)|^2$. In performing the integral in (2.5) we again replace $N_f^* \int_{FS} d^2s\, n(s)$ by $N_f \int_{\Omega_c} d\varphi \theta d\theta / 4\pi$. This yields only a z-component to the nonlinear current,

$$j_{nl,z} = -\frac{eN_f v_f \Delta_p}{2\pi} \int_0^{2\pi} d\varphi \int_0^{\theta_c} \theta d\theta (\theta_c^2 - \theta^2)^{1/2} \Theta(v_z - v_s), \tag{A5}$$

where $\theta_c^2 \equiv [(v_f v_z)^2 - \Delta_{\min}^2]/\Delta_p^2$. We get,

$$j_z = \frac{e\rho}{v_p^2} \left(v_z^2 - v_s^2\right)^{3/2} \Theta(v_z - v_s), \tag{A6}$$

where $v_p \equiv \Delta_p / v_f$, $v_s \equiv \Delta_{\min}/v_f$, and, in three dimensions, $\rho \equiv \frac{1}{3} N_f v_f^2$. The step function reflects that the flow field v_z must be sufficiently large, $v_z > v_s$, in order for nonlinear effects to be present.

b. 3-D line quasinode

For an energy gap as given in (3.22), where the nodal line is at $\theta = \pi/2$, $v_{fz} = 0$ over the region of integration, which is then limited to $|\theta - \pi/2| < \theta_c$. Here $(\theta_c - \pi/2)^2 = \left[(\mathbf{v}_f \cdot \mathbf{v})^2 - \Delta_{\min}^2\right]/\Delta_p^2 = \left[(v_f v_\perp \cos\eta)^2 - \Delta_{\min}^2\right]/\Delta_p^2$, where $v_\perp = (v_x^2 + v_y^2)^{1/2}$ is the projection of $\mathbf{v}$ on the $x - y$ plane, and η the angle between $v_\perp$ and the in-plane v_f. In our geometry $v_y = 0$ and the only component of the nonlinear contribution to the current is along x. We have,

$$j_{nl,x} = \frac{eN_f v_f \Delta_p}{2\pi} \int_{\varphi_1}^{\varphi_2} \int_{-\theta_c}^{\theta_c} d\varphi d\theta v_f \cos\varphi (\theta_c^2 - \theta^2)^{1/2} \Theta(v_\perp - v_s). \tag{A7}$$

After performing the integration over θ, this leaves an integral over φ. To find the specific limits in this integral, we transform the integral over φ to one over η. Using the relation $\varphi = \beta + \eta$, where β is the (fixed) angle $v_\perp$ makes with the x axis, we find,

$$j_{nl,x} = \frac{eN_f v_f}{4\Delta_p} \int_{-\varphi_s}^{\varphi_s} d\eta \cos(\beta + \eta) [(v_f v_\perp \cos\eta)^2 - \Delta_{\min}^2] \Theta(v_\perp - v_s), \tag{A8}$$

where $\varphi_s = \arccos(-\Delta_{\min}/v_f v_\perp)$. Making use of $\cos\beta = v_x/v_\perp$, we get the nonlinear contribution to the current:

$$j_{nl,x} = \frac{e\rho}{v_p v_\perp^2} v_x \left(v_\perp^2 - v_s^2\right)^{3/2} \Theta(v_\perp - v_s). \tag{A9}$$

APPENDIX B: PERTURBATION SOLUTION

1. 2-D YBCO-type orthorhombicity

Here we assume that the anisotropy factor, $\Lambda_a > 1$, and first examine the case when $\psi \in [\psi_1, \psi_2]$, where the limiting angles ψ_i are defined in the text. We will need their expressions in the slab limit, $d \gg \lambda$, which are:

$$\psi_1 = \tan^{-1}\left(\frac{\tan\alpha\, e^{\zeta_{s,a}(1-\Lambda_a)}}{\Lambda_a}\right), \tag{B1a}$$

$$\psi_2 = \tan^{-1}\left(\frac{\tan\alpha}{\Lambda_a}\right). \tag{B1b}$$

However, unless otherwise stated, all expressions below are for arbitrary d. Without loss of generality, we give details of the solution for the a-component of the nonlinear current, and simply give the results for the b-component later, since it follows from an identical procedure. We find after inserting (A3a) into (2.7),

$$\frac{d^2u_a}{d\zeta_a^2} - u_a - 2\varepsilon u_a u_b \cos\alpha\sin\alpha = 0, \qquad \zeta_a \in [\zeta_a^*, \zeta_{s,a}] \tag{B2a}$$

$$\frac{d^2u_a}{d\zeta_a^2} - u_a + \varepsilon[u_a^2 \cos^2\alpha + u_b^2 \sin^2\alpha] = 0, \qquad \zeta_a \in [0, \zeta_a^*] \tag{B2b}$$

Here $\varepsilon = \Lambda_{a,n}^2 (H_A/H_0)\cos\alpha$, $\Lambda_{i,n} = \lambda_i/\lambda_n$ (for $i = a, b$), $\lambda_n^{-2} \equiv \frac{2\pi e^2}{c^2} N_f v_f^2$. We can now solve Eqs. (B2a) and (B2b) perturbatively in the small parameter ε, and write $u_i = u_{0,i} + \varepsilon u_{1,i}$. To zeroth order, we have $u_{0,a} = \Lambda_a^{1/2} \sin\psi\,\mathrm{sech}(\zeta_{s,a})\sinh(\zeta_a)$, and $u_{0,b} = -\Lambda_b^{1/2}\cos\psi\,\mathrm{sech}(\zeta_{s,b})\sinh(\zeta_b)$, where $\Lambda_b \equiv \lambda_b/\lambda_a$. The first order solutions satisfy the following two equations:

$$\frac{d^2u_{1,a}}{d\zeta_a^2} - u_{1,a} - 2\,u_{0,a}u_{0,b} \cos\alpha\sin\alpha = 0, \qquad \zeta_a \in [\zeta_a^*, \zeta_{s,a}] \tag{B3a}$$

$$\frac{d^2u_{1,a}}{d\zeta_a^2} - u_{1,a} + [u_{0,a}^2 \cos^2\alpha + u_{0,b}^2 \sin^2\alpha] = 0, \qquad \zeta_a \in [0, \zeta_a^*]. \tag{B3b}$$

The boundary condition on the nonlinear terms is $\partial u_{1i}/\partial\zeta_i|_{\zeta_{s,i}} = 0$. By requiring continuity of the flow field, current, and magnetic field at the point ζ_a^*, we can obtain the first order solution $u_{nl,a} = \varepsilon u_{1,a}$ to (B3a):

$$u_{nl,a} = \Lambda_{a,n}^2 \cos\alpha \frac{H_A}{H_0}\Big[C_{1a}\cosh(\zeta_a) + C_{2a}\sinh(\zeta_a) + w_a(\zeta_a)\cosh(\zeta_a) + g_a(\zeta_a)\sinh(\zeta_a)\Big]. \tag{B4}$$

Here the constants C_{1i} and C_{2i} are given by $C_{1i} = \overline{w}_i(\zeta_i^*) - \overline{w}_i(0) - w_i(\zeta_i^*)$, $C_{2i} = -g_i(\zeta_{s,i}) + \tanh(\zeta_{s,i})[\overline{w}_i(0) + w_i(\zeta_i^*) - w_i(\zeta_{s,i}) - \overline{w}_i(\zeta_i^*)]$, with $\overline{w}_a \equiv -\mu_2 U_a - \mu_3 W_{c,a}$, $w_a \equiv -\mu_1 G_{c,a}$, $g_a \equiv \mu_1 G_{s,a}$, and

$$G_{s,i}(\zeta_i) = \frac{\sinh((\Lambda_i+2)\zeta_i)}{4(\Lambda_i+2)} - \frac{\sinh((\Lambda_i-2)\zeta_i)}{4(\Lambda_i-2)}, \tag{B5a}$$

$$G_{c,i}(\zeta_i) = \frac{\cosh((\Lambda_i+2)\zeta_i)}{4(\Lambda_i+2)} + \frac{\cosh((\Lambda_i-2)\zeta_i)}{4(\Lambda_i-2)} - \frac{\cosh(\Lambda_i\,\zeta_i)}{2\Lambda_i}, \tag{B5b}$$

$$W_{c,i}(\zeta_i) = \frac{\cosh((2\Lambda_i+1)\zeta_i)}{4(2\Lambda_i+1)} - \frac{\cosh((2\Lambda_i-1)\zeta_i)}{4(2\Lambda_i-1)} - \frac{\cosh(\zeta_i)}{2}, \tag{B5c}$$

$$U_i(\zeta_i) = \frac{1}{12}\cosh(3\,\zeta_i) - \frac{3}{4}\cosh(\zeta_i), \tag{B5d}$$

$$\mu_1 = -\frac{\sin 2\alpha\sin 2\psi}{2\cosh(\zeta_{s,a})\cosh(\zeta_{s,b})}, \tag{B5e}$$

$$\mu_2 = -\frac{\Lambda_a\cos^2\alpha\sin^2\psi}{\cosh^2(\zeta_{s,a})}, \tag{B5f}$$

$$\mu_3 = -\frac{\Lambda_b\sin^2\alpha\sin^2\psi}{\cosh^2(\,\zeta_{s,b})}. \tag{B5g}$$

Similarly, (B3b) gives

$$u_{1,a} = C_{3a}\cosh(\zeta_a) + C_{4a}\sinh(\zeta_a) + \overline{w}_a(\zeta_a)\cosh(\zeta_a) + \overline{g}_a(\zeta_a)\sinh(\zeta_a), \tag{B6}$$

where $C_{3i} = -\overline{w}_i(0), C_{4i} = C_{2i} + g_i(\zeta_i^*) - \overline{g}_i(\zeta_i^*)$. Here $\overline{g}_a \equiv \mu_2 V_a + \mu_3 W_{s,a}$, and

$$W_{s,i}(\zeta_i) = \frac{\sinh((2\Lambda_i-1)\zeta_i)}{4(2\Lambda_i-1)} + \frac{\sinh((2\Lambda_i+1)\zeta_i)}{4(2\Lambda_i+1)} - \frac{\sinh(\zeta_i)}{2}, \tag{B7}$$

$$V_i(\zeta_i) = \frac{1}{4}\sinh(\zeta_i) - \frac{1}{12}\sinh(3\zeta_i). \tag{B8}$$

The matching point ζ_a^* (for $\zeta_{s,a} \gg 1$) is :

$$\zeta_a^* = \zeta_{s,a} - \frac{1}{1-\Lambda_a} \ln\left(\frac{\Lambda_a \tan\psi}{\tan\alpha}\right). \tag{B9}$$

The b-component is found by a similar procedure. We find,

$$u_{nl,b} = \Lambda_{b,n}^2 \sin\alpha \frac{H_A}{H_0}\Big[C_{1b}\cosh(\zeta_b) + C_{2b}\sinh(\zeta_b) + w_b(\zeta_b)\cosh(\zeta_b) + g_b(\zeta_b)\sinh(\zeta_b)\Big], \tag{B10}$$

$$\zeta_b \in [\zeta_b^*, \zeta_{s,b}],$$

$$u_{nl,b} = \Lambda_{b,n}^2 \sin\alpha \frac{H_A}{H_0}\Big[C_{3b}\cosh(\zeta_b) + C_{4b}\sinh(\zeta_b) + \overline{w}_b(\zeta_b)\cosh(\zeta_b) + \overline{g}_b(\zeta_b)\sinh(\zeta_b)\Big], \tag{B11}$$

$$\zeta_b \in [0, \zeta_b^*],$$

where, $w_b = \mu_2 W_{c,b} + \mu_3 U_b$, $g_b = -\mu_2 W_{s,b} - \mu_3 V_b$, $\overline{w}_b = \mu_1 G_{c,b}$, and $\overline{g}_b = -\mu_1 G_{s,b}$.

The fields calculated above are for $\psi \in [\psi_1, \psi_2]$. For $\psi \in [0, \psi_1]$, we get $u_{nl,i}$ by simply setting the crossover point $\zeta_i^* = 0$ in Eqs. (B4,B10). Similarly, to find the nonlinear fields for $\psi \in [\psi_2, \pi/2]$, we set $\zeta_i^* = \zeta_{s,i}$ in Eqs. (B6,B12).

2. 3-D quasi-nodes

a. 3-D point quasinodes

For the geometry we consider, $\mathbf{H}_\mathrm{A}$ is in the $a-c$ plane, and the nonlinear fields now have only a z-component, which depends on the coordinate y. The flow field decreases rapidly with distance into the sample, so that there will be a point in the material, ζ_z^*, where $u_z < \kappa$, so that nonlinear corrections are absent for distances below ζ_z^*. Again, there is no restriction on sample thickness, unless otherwise stated. Inserting the current (A6) into (2.7) gives:

$$\frac{d^2 u_z}{d\zeta_z^2} - u_z + \varepsilon\left(u_z^2 - \kappa^2\right)^{3/2} \Theta(u_z - \kappa) = 0, \tag{B12a}$$

where $\varepsilon \equiv h^2 = (H_A/H_0)^2$, and κ and H_0 are defined in the text. (B12a) can be written as

$$\frac{d^2 u_z}{d\zeta_z^2} - u_z + \varepsilon(u_z^2 - \kappa^2)^{3/2} = 0, \qquad \zeta_z \in [\zeta_z^*, \zeta_{s,z}], \tag{B13a}$$

$$\frac{d^2 u_z}{d\zeta_z^2} - u_z = 0, \qquad \zeta_z \in [0, \zeta_z^*]. \tag{B13b}$$

We now solve (B13a) perturbatively to first order, and write $u_{nl,z} = \varepsilon\, u_{1z}$. We find,

$$u_{nl,z}(\zeta_z) = \frac{H_A^2}{H_0^2}[D_1\cosh(\zeta_z) + D_2\sinh(\zeta_z) + k(\zeta_z)\cosh(\zeta_z) + f(\zeta_z)\sinh(\zeta_z)], \tag{B14}$$

where the constants D_1 and D_2 are found by requiring continuity of the fields at ζ_z^*, and given by $D_1 = -k(\zeta_z^*)$, $D_2 = -f(\zeta_{s,z}) + \tanh(\zeta_{s,z})[k(\zeta_z^*) - k(\zeta_{s,z})]$. The functions f and k are found by elementary methods, and are given by,

$$\begin{aligned} f(\zeta_z) = \frac{1}{8}\Bigg(&-\frac{3\kappa^4}{m(\psi)} \ln\left[2\left(m(\psi)\sinh(\zeta_z) + \sqrt{m^2(\psi)\sinh^2(\zeta_z) - \kappa^2}\right)\right] \\ &+ \left[5\kappa^2\sinh(\zeta_z) - 2m^2(\psi)\sinh^3(\zeta_z)\right]\left[m^2(\psi)\sinh^2(\zeta_z) - \kappa^2\right]^{1/2}\Bigg)\Theta\Big(m(\psi)\sinh(\zeta_z) - \kappa\Big), \end{aligned} \tag{B15a}$$

$$\begin{aligned} k(\zeta_z) = \frac{1}{8}\Bigg(&\frac{3}{m(\psi)}(m^2(\psi) + \kappa^2)^2 \ln\left[\sqrt{2}\left(m(\psi)\cosh(\zeta_z) + \sqrt{m^2(\psi)\sinh^2(\zeta_z) - \kappa^2}\right)\right] \\ &+ \cosh(\zeta_z)\left[-4m^2(\psi) - 5\kappa^2 + m^2(\psi)\cosh(2\zeta_z)\right] \\ &\times \left[m^2(\psi)\sinh^2(\zeta_z) - \kappa^2\right]^{1/2}\Bigg)\Theta\Big(m(\psi)\sinh(\zeta_z) - \kappa\Big), \end{aligned} \tag{B15b}$$

where $m(\psi) \equiv \sin\psi/\cosh\zeta_{s,z}$. The matching point is found to be $\zeta_z^* = \sinh^{-1}[\kappa/m(\psi)]$. In a similar fashion, (B13b) has the first order solution

$$u_{1z} = [f(\zeta_z^*) - f(\zeta_{s,z}) + \tanh(\zeta_{s,z})(k(\zeta_z^*) - k(\zeta_{s,z}))]\sinh(\zeta_z). \tag{B16}$$

b. 3-D line quasinode.

$\mathbf{H}_{\mathrm{A}}$ is again in the $a-c$ plane, and due to the form of the gap, the nonlinear fields now have only a x-component, which depends on the coordinate y. Here $u_x > \kappa$, in order for nonlinear effects to be present. These effects are therefore absent at distances below ζ^*. Inserting (A9) into (2.7) gives the following:

$$\frac{d^2u_x}{d\zeta^2} - u_x + \frac{\varepsilon}{u_x}\left(u_x^2 - \kappa^2\right)^{3/2}\Theta(u_x - \kappa) = 0, \tag{B17}$$

where the small parameter ε is $\varepsilon \equiv h \equiv H_A/H_0$.

We can now solve (B17) perturbatively to first order. We write $u_x = u_{0x} + \varepsilon u_{1x}$. To avoid unnecessarily tedious calculations, we take the slab limit, and hence the zeroth order solution, u_{0x} is, $u_{0x} \approx -\cos\psi\exp(\zeta - \zeta_s)$. The first order solution, u_{1x}, is found from dividing the slab at ζ^* into two portions. This allows (B17) to be written

$$\frac{d^2u_x}{d\zeta^2} - u_x + \frac{\varepsilon}{u_x}\left(u_x^2 - \kappa^2\right)^{3/2} = 0, \qquad \zeta \in [\zeta^*, \zeta_s], \tag{B18a}$$

$$\frac{d^2u_x}{d\zeta^2} - u_x = 0, \qquad \zeta \in [0, \zeta^*]. \tag{B18b}$$

The solution to (B18a) is found by methods similar to the point node case, and is given by

$$u_{1x} = E_1\, e^{\zeta} + E_2\, e^{-\zeta} + r(\zeta)\, e^{\zeta} + s(\zeta)\, e^{-\zeta}, \tag{B19}$$

The functions $r(\zeta)$ and $s(\zeta)$ are found by elementary methods, and the constants E_1 and E_2 are determined from the boundary conditions $(\partial u_{1x}/\partial\zeta)|_{\zeta_s} = 0$, and continuity of the flow field, current, and magnetic field at the point ζ^*:

$$E_1 = (s(\zeta_s) - s(\zeta^*) - r(\zeta^*))e^{-2\zeta_s} + r(\zeta_s) \tag{B20a}$$

$$E_2 = -s(\zeta_s)e^{-2\,\zeta_s} + r(\zeta_s) - s(\zeta^*) - r(\zeta^*) \tag{B20b}$$

$$\begin{aligned} r(\zeta) = \frac{1}{8}\Bigg[&-3n(\psi)\kappa\tan^{-1}\left(\frac{n^2(\psi)\, e^{2\,\zeta} - 2\kappa^2}{2\kappa\,\sqrt{n^2(\psi)\, e^{2\,\zeta} - \kappa^2}}\right) \\ &+ \frac{2}{n(\psi)}(2\, n^2(\psi) + \kappa^2 e^{-2\zeta})\sqrt{n^2(\psi)e^{2\zeta} - \kappa^2}\Bigg]\Theta\left(n(\psi)e^{\zeta} - \kappa\right), \end{aligned} \tag{B20c}$$

$$\begin{aligned} s(\zeta) = \frac{1}{6}\Bigg[&-\frac{3\kappa^3}{n(\psi)}\tan^{-1}\left(\frac{\sqrt{n^2(\psi)\, e^{2\zeta} - \kappa^2}}{\kappa}\right) \\ &+ \frac{1}{n(\psi)}(4\kappa^2 - n^2(\psi)\, e^{2\zeta})\sqrt{n^2(\psi)e^{2\zeta} - \kappa^2}\Bigg]\Theta\left(n(\psi)e^{\zeta} - \kappa\right), \end{aligned} \tag{B20d}$$

where $n(\psi) \equiv \cos\psi\exp(-\zeta_s)$. Similarly, (B18b) can be solved, with the only major difference begin the boundary condition $u_{1x}(0) = 0$. We find,

$$u_{1x} = E_3\left(e^{\zeta} - e^{-\zeta}\right), \tag{B21}$$

where

$$E_3 = (s(\zeta_s) - s(\zeta^*))e^{-2\,\zeta_s} - r(\zeta_s) + r(\zeta^*). \tag{B22}$$

The matching point ζ^* is found by equating (B18a) and (B18b) at ζ^*, giving $\zeta^* = \zeta_s + \ln[\kappa/\cos\psi]$.

---

[*] Electronic address: khalter@physics.umn.edu

[†] Electronic address: otvalls@tc.umn.edu

[‡] Electronic address: igor@cooperon.umd.edu

[1] See however: R. Balian and N.R. Werthamer, Phys. Rev. **131**, 1553 (1963); L.J. Buchholtz and G. Zwicknagl, Phys. Rev. B **23**, 5788 (1981).
[2] A.J. Leggett, Rev. Mod. Phys. **47**, 331 (1975). J. C. Wheatley, *ibid* 415 (1975).
[3] J.F. Annett, N. Goldenfeld and A.J. Leggett, in *Physical properties of high temperature superconductors V*, D.M. Ginzburg, ed., World Scientific, Singapore (1996).
[4] C.C. Tsuei and J.R. Kiertley, cond-mat/0004185 (2000).
[5] M. Franz and Z. Tešanović, Phys. Rev. Lett. **80**, 4763 (1998); M. Mößle and R. Kleiner, Phys. Rev. **B59**, 4486, (1999); Q. Li *et al*, Phys. Rev. Lett. **83**, 4160, (1999).
[6] S.M. Anlage *et al.* Phys. Rev. B **50**, 523 (1994); J.D. Kokales *et al.*, cond-mat/0002300; R. Prozorov *et al.*, cond-mat/0002301.
[7] J.A. Sauls, Adv. Phys. **43**, 113 (1994).
[8] A. Amato, Rev. Mod. Phys. **69**, 1119 (1997).
[9] K. Machida, T. Nishira, and T. Ohmi, cond-mat/9906105.
[10] R. Lal and S.K. Joshi, Phys. Rev. B **41**, 1894, (1990).
[11] K. Kanoda, K. Miyagawa, A. Kawamoto, and Y. Nakazawa Phys. Rev. **B54**, 76, (1996).
[12] L.P. Le *et al.*, Phys. Rev. Lett. **68**, 1923 (1992).
[13] A. G. Lebed, Phys. Rev. B **59**, R721 (1999)
[14] K. Kanoda, K. Akiba, K. Suzuki, and T. Takahashi, Phys. Rev. Lett. **65**, 1271 (1990).
[15] A. Carrington *et al.*, Phys. Rev. Lett. **83**, 4172 (1999).
[16] T. Ishiguro, K. Yamaji, and G. Saito, *Organic Superconductors* (Springer, Berlin, 1998).
[17] Y. Maeno *et al.*, Nature **372**, 532 (1994).
[18] I.I. Mazin and D.J. Singh, Phys. Rev. Lett. **79**, 733 (1997).
[19] T.M. Riseman *et al.*, Nature **396**, 242 (1998).
[20] K. Ishida *et al.*, Nature **396**, 658 (1998).
[21] M. Matsumoto and M. Sigrist, cond-mat/9903004.
[22] G.M. Luke *et al.*, Nature **394**, 558 (1998).
[23] M. Sigrist *et al.*, cond-mat/9902214.
[24] H. Kee, Y. Kim, K. Maki, cond-mat/9907276.
[25] M. Rice, Nature **396**, 627 (1998).
[26] T. Dahm, H.Won, and K. Maki, cond-mat/0006301.
[27] W.N. Hardy, D.A. Bonn, D.C. Morgan, R. Laing and K. Zhang, Phys. Rev. Lett. **70**, 3999 (1993). Initial interest focused on the temperature dependence of λ (without resolving its angular dependence), which provided strong support for unconventional superconductivity in HTSC's.
[28] S.K. Yip and J.A. Sauls, Phys. Rev. Lett. **69**, 2264 (1992).
[29] B.P. Stojković and O.T. Valls, Phys. Rev. B **51**, 6049, (1995).
[30] D. Xu, S.K. Yip and J.A. Sauls, Phys. Rev. B **51**, 16233, (1995).
[31] I. Žutić and O.T. Valls, Phys. Rev. B **54**, 15500, (1996).
[32] T. Dahm and D.J. Scalapino, J. Appl. Phys. **81**, 2002 (1997); Appl. Phys. Lett. **69**, 4248 (1996).
[33] M.H.S. Amin *et al.*, Phys. Rev. B **58**, 5848 (1998).
[34] I. Žutić and O.T. Valls, Phys. Rev. B **56**, 11279, (1997).
[35] A. Bhattacharya *et al.* Phys. Rev. Lett. **82**, 3132, (1999).
[36] C. Bidinosti and W. Hardy, Phys. Rev. Lett. **83**, 3277 (1999).
[37] K. Halterman and O.T. Valls, Phys. Rev. B, in press, cond-mat/0003247.
[38] T.P. Orlando and K. A. Delin, *Foundations of Applied Superconductivity* (Addison-Wesley, Reading, MA, 1991)
[39] M. Tinkham, *Introduction to Superconductivity* (McGraw-Hill, New York, 1974)
[40] C. Bidinosti, private communication.
[41] A.L. Fetter and J.D. Walecka *Quantum Theory of Many-Particle Systems* (McGraw-Hill, New York, 1971).
[42] J.D. Jackson, *Classical Electrodynamics* (Wiley, New York, 1975).
[43] I. Žutić and O.T. Valls, J. Comput. Phys. **136**, 337 (1997); J. Appl. Phys. **83**, 6804 (1998).
[44] E. Schachinger and J.P. Carbotte, Phys. Rev. B **60**, 12 400 (1999).
[45] In Ref. 34, the customary distinction between the presence of an s wave gap and FS anisotropy was kept. We have here eliminated this distinction and recalculated the fields in terms of the best minimum set of variables.
[46] The angles ϕ_1 can be inferred from photoemission or other experiments.
[47] A. Carrington, R.W. Giannetta, J.T. Kim and J. Giapintzakis, Phys. Rev. B **59**, R14173 (1999).
[48] D.N. Basov, *et al.* Phys. Rev. Lett. **74**, 598, (1995).
[49] M.-R. Li, P.J. Hirschfeld, and P. Wölfle, Phys. Rev. Lett. **81**, 5640 (1998); I. Kostzin and A.J. Leggett, Phys. Rev. Lett. **81**, 5640 (1998).
[50] A. Bhattacharya *et al.*, Phys. Rev. Lett. **83**, 887 (1999).
[51] W.A. Atkinson *et al.* cond-mat/0005487
[52] Y.T. Wang, and A.M. Hermann, preprint.
[53] I. Žutić and O.T. Valls, Phys. Rev. B **58**, 8738 (1998).

[54] T. Dahm and D.J. Scalapino, Phys. Rev. B **60**, 13 125 (1999).
[55] S.M. Anlage, private communication.

FIG. 1. Variables and labels for the OP in subsection III A. The four nodal lines are labeled by the numbers (1) through (4). The Fermi velocity at node (1), $\mathbf{v}_f$, forms an angle α with the a-axis. The applied field $\mathbf{H}_\mathrm{A}$ is at an angle ψ to the a-axis. A generic flow field vector $\mathbf{v}$ is shown for illustrative purposes.

FIG. 2. Angular dependence of $\Delta\lambda$ for the OP in subsection III A, with YBCO-type orthorhombicity. We plot here the function $\mathcal{Y}(\psi)$ (Eqs. 3.9a-3.9c), vs. the angle ψ. This function represents the angular dependence of $\Delta\lambda$ normalized by the field dependence and numerical prefactors in (3.8). In this Figure, the Fermi velocity direction is fixed at an angle $\alpha = \pi/4$. The bolder line shows the result for the orthorhombicity parameter $\Lambda_a \equiv \lambda_a/\lambda_b = 1.0$ (tetragonal limit), while Λ_a equals 1.1, 1.2, 1.3, 1.4 and 1.5 in the other curves (from top to bottom at $\psi = 0$).

FIG. 3. Angular dependence of $\Delta\lambda$, for the same OP as in Fig. 2. Again, the function $\mathcal{Y}(\psi)$ is plotted. Here $\Lambda_a = 1.0$ is fixed, while α takes the values $\pi/4 \pm n(\pi/80)$ with $n = 0, 1, 2, 3$. As in the previous Figure, the effect of orthorhombicity is quite strong. The bold line is the tetragonal ($n = 0$) case. The positive values of n are (dotted curves) above the bold curve at small angles, and those for negative n (dashed) are below.

FIG. 4. Angular dependence of $\Delta\lambda$ for the same OP as in Figs. 2 and 3. Here $\Lambda_a = 1.3$ is fixed, while α takes the same values as in the previous Figure. The solid curve corresponds to $\alpha = \pi/4$ and the meaning of the dotted and dashed lines is as in the previous Figure. The combined effects of the two anisotropy parameters are seen.

FIG. 5. Angular dependence of $\Delta\lambda$ for a 2-D OP with line nodes and BSCCO-type orthorhombicity (subsection III B). The applied field makes an angle ψ with the new orthorhombic a-axis. The nodal lines are now along the principal axes, which are rotated by an angle of $\pi/4$ relative to the previous undistorted tetragonal axes. The curves are normalized so that they represent the function $\mathcal{B}(\psi)$ as defined in (3.11). They correspond, from top to bottom at $\psi = 0$ to values of $\Lambda_a = 1.0, 1.1, 1.2, 1.3, 1.4, 1.5$. As in previous Figures, the tetragonal limit is plotted with a bolder line.

FIG. 6. Angular dependence of $\Delta\lambda$ for a 2-D gap with quasinodes and tetragonal symmetry as discussed in subsection III C. Results are normalized so that the quantity plotted is the function $\mathcal{Q}$ of (3.15). This function is plotted vs. the angle ψ that the applied field forms with the a axis. The bolder line corresponds to the usual result with nodes, ($\kappa = 0$ see (3.13)), and the other curves, from top to bottom, are for values of κ of 0.2, 0.4, 0.6 and 0.8 respectively.

FIG. 7. Field dependence of $\Delta\lambda(\psi)$ for the same 2-D gap with line quasinodes considered in the previous Figure. The curves show the quantity $\Delta\lambda/\lambda$ (see 3.14) at $\psi = \pi/4$, as a function of h for values of δ (see text) equal to 0, 0.01, 0.02, 0.03, 0.04 and 0.05 These values can be read off from the threshold field values in the curves.

FIG. 8. Angular and field dependence of $\Delta\lambda(\psi)$ for a 3-D gap with point quasinodes. The main plot is normalized so that the quantity plotted is the function $\mathcal{P}(\psi, \kappa)$ defined in (3.19). This quantity is plotted as a function of angle for values of $\kappa = 0, 0.1, 0.2, 0.3, 0.4, 0.6, 0.8$, as defined in (3.21). The bolder curve is the $\kappa = 0$ result. The inset displays the field dependence of $\Delta\lambda$ at $\psi = \pi/2$. The quantity plotted is $\Delta\lambda/\lambda_z$ vs. normalized applied field, for values of δ equal to 0, 0.01, 0.02, 0.03, 0.04 and 0.05.

FIG. 9. Angular dependence of $\Delta\lambda(\psi)$ for a 3-D line quasinode. The main plot is normalized so that the quantity plotted is the function $\mathcal{L}(\psi, \kappa)$ defined in (3.25). The inset has the field dependence of $\Delta\lambda$ at $\psi = 0$. All parameter values are precisely as in the previous Figure.

Halterman and Valls Fig.1

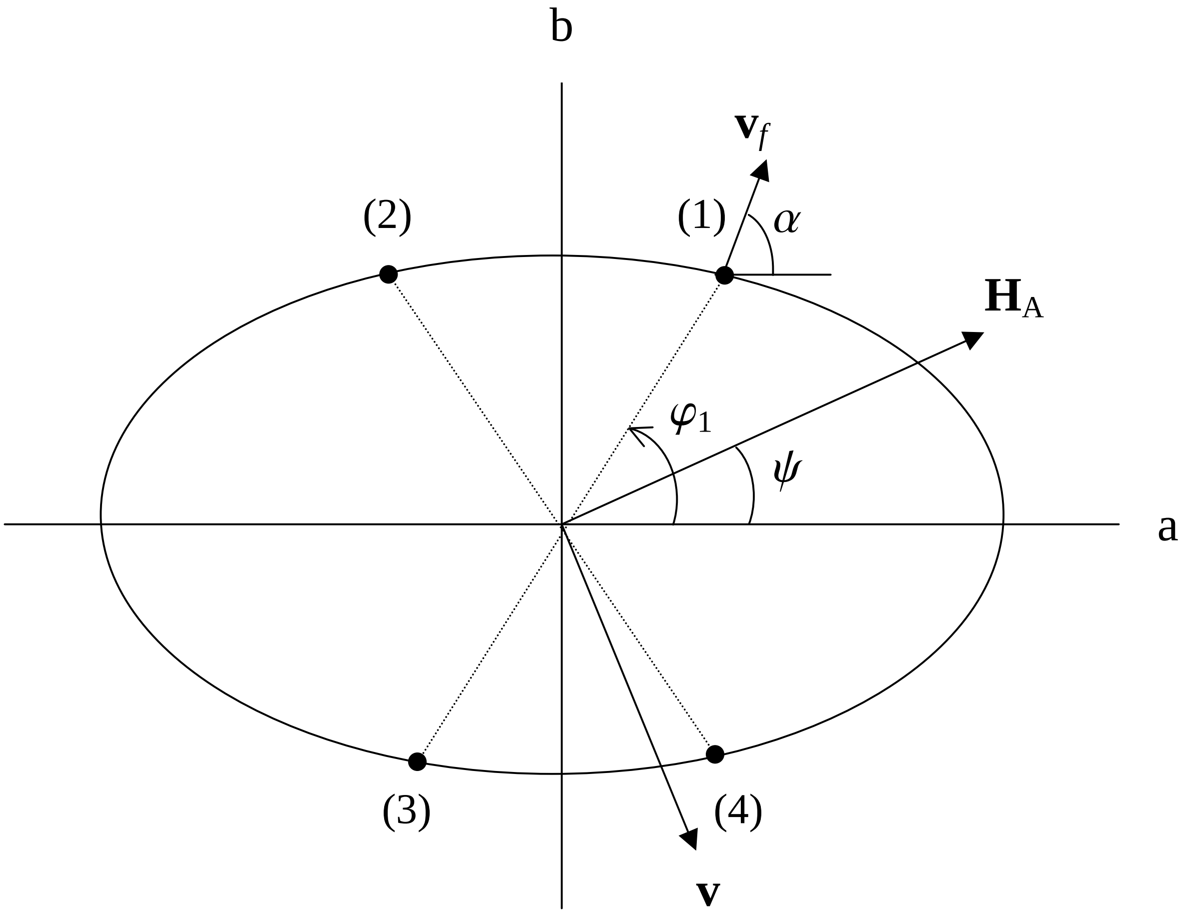

Halterman and Valls Fig.2

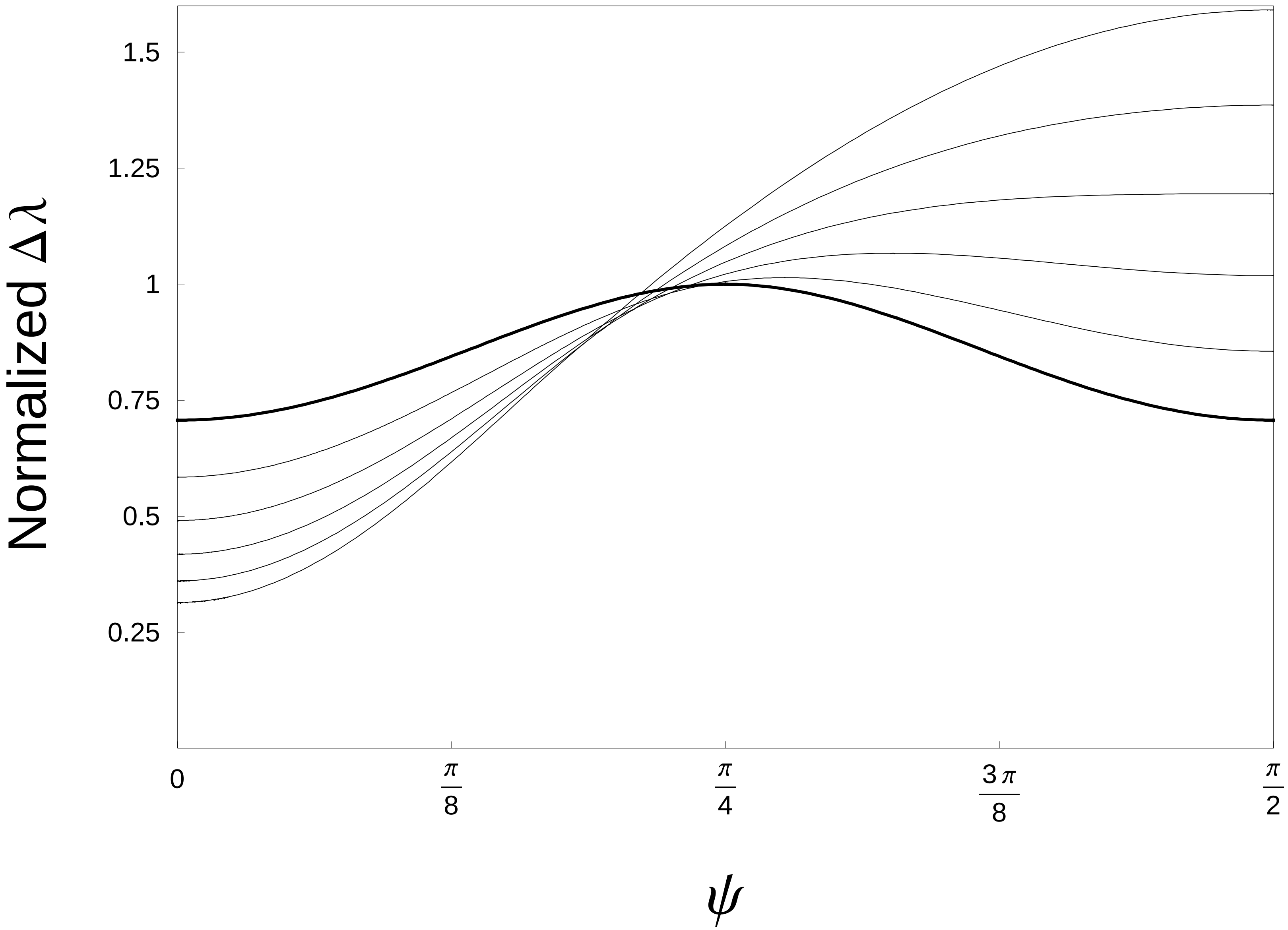

Halterman and Valls Fig.3

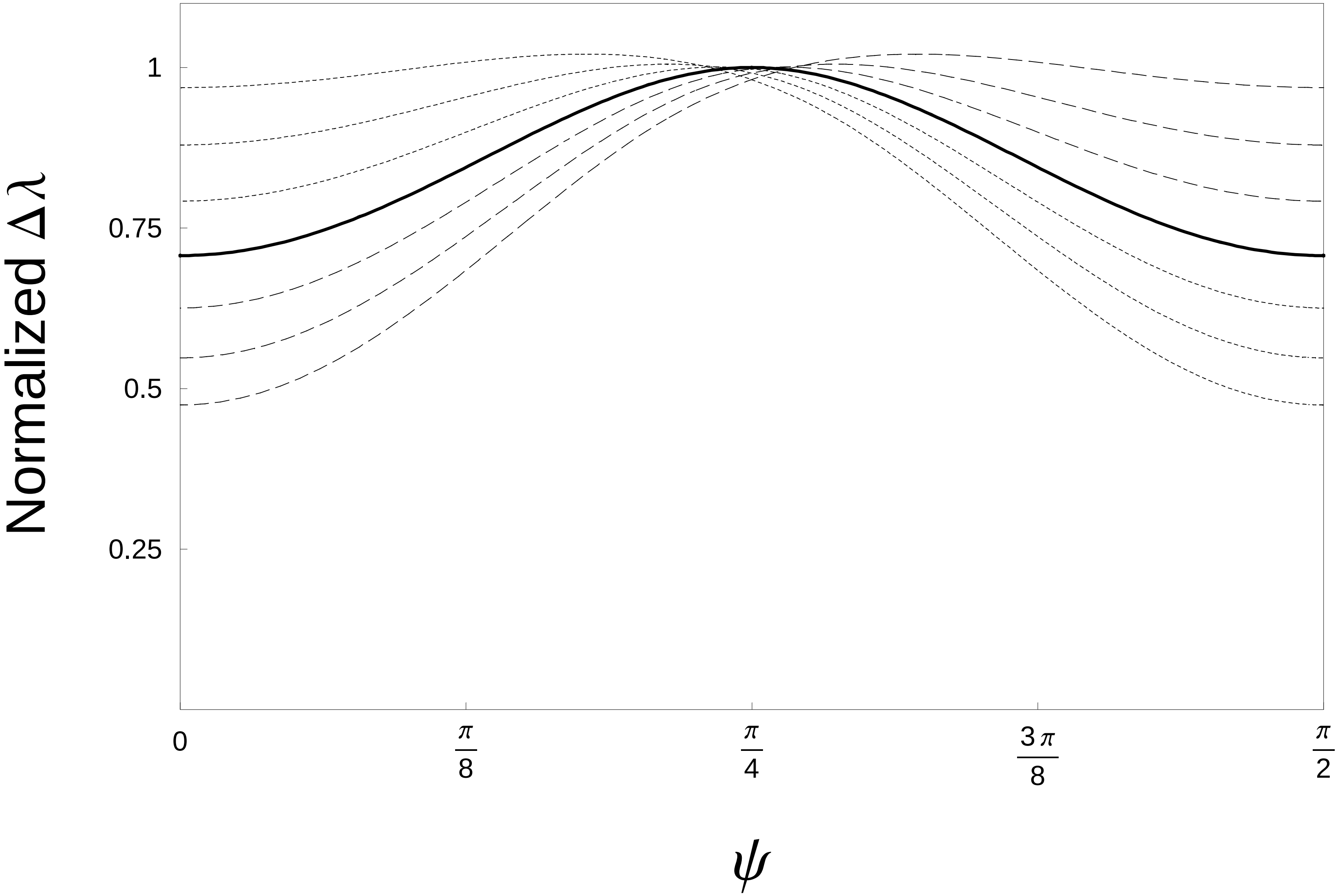

Halterman and Valls Fig.4

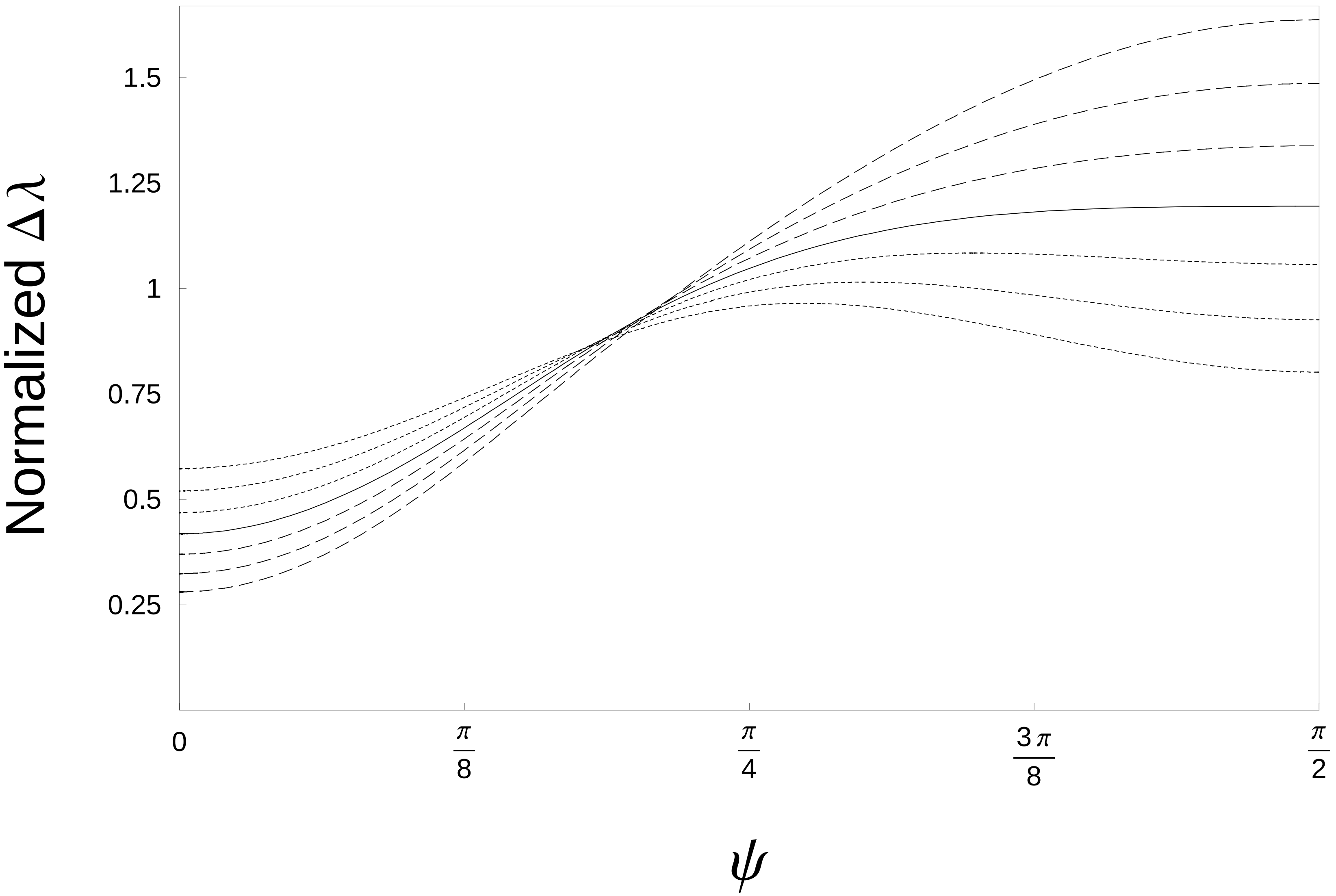

Halterman and Valls Fig.5

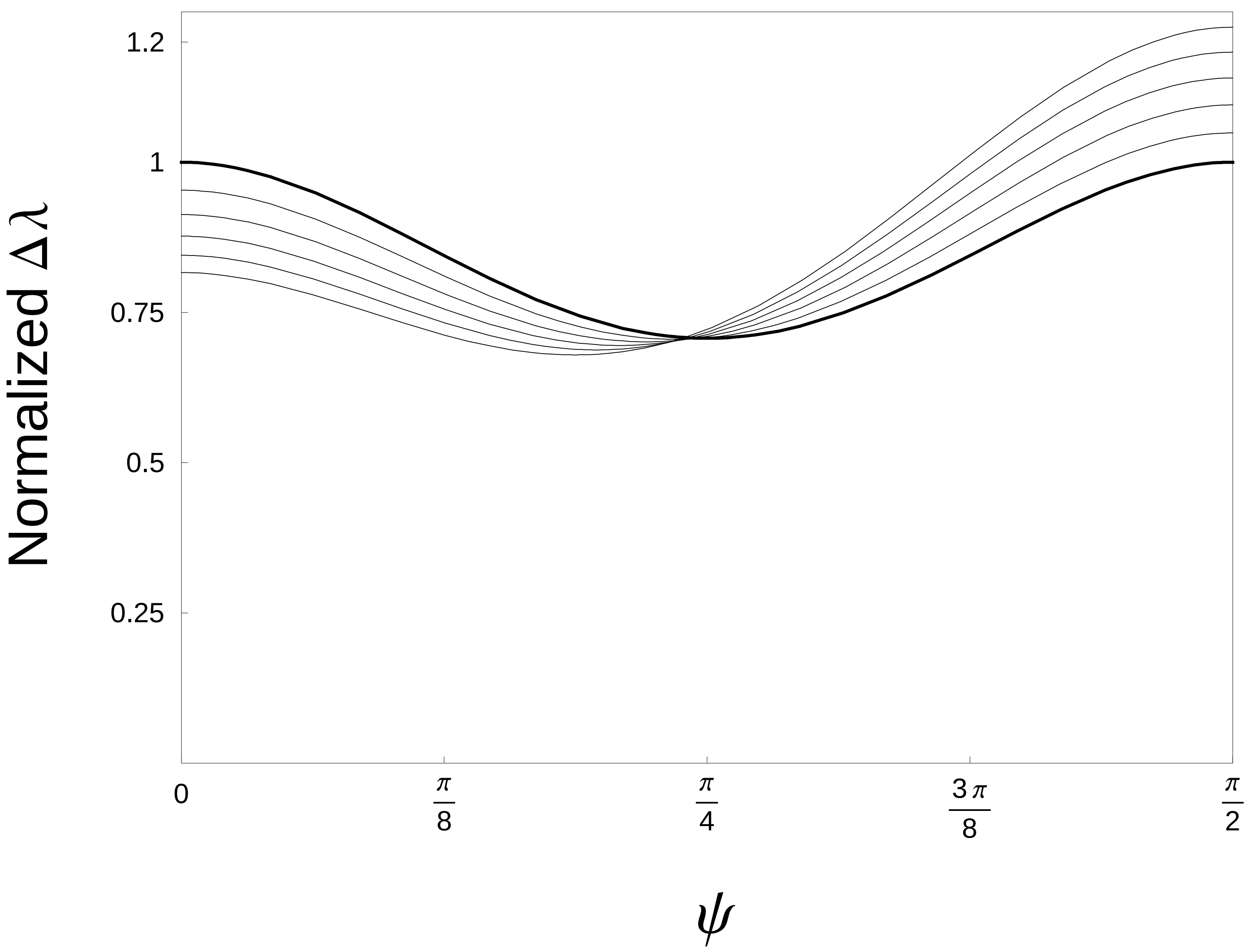

Halterman and Valls Fig.6

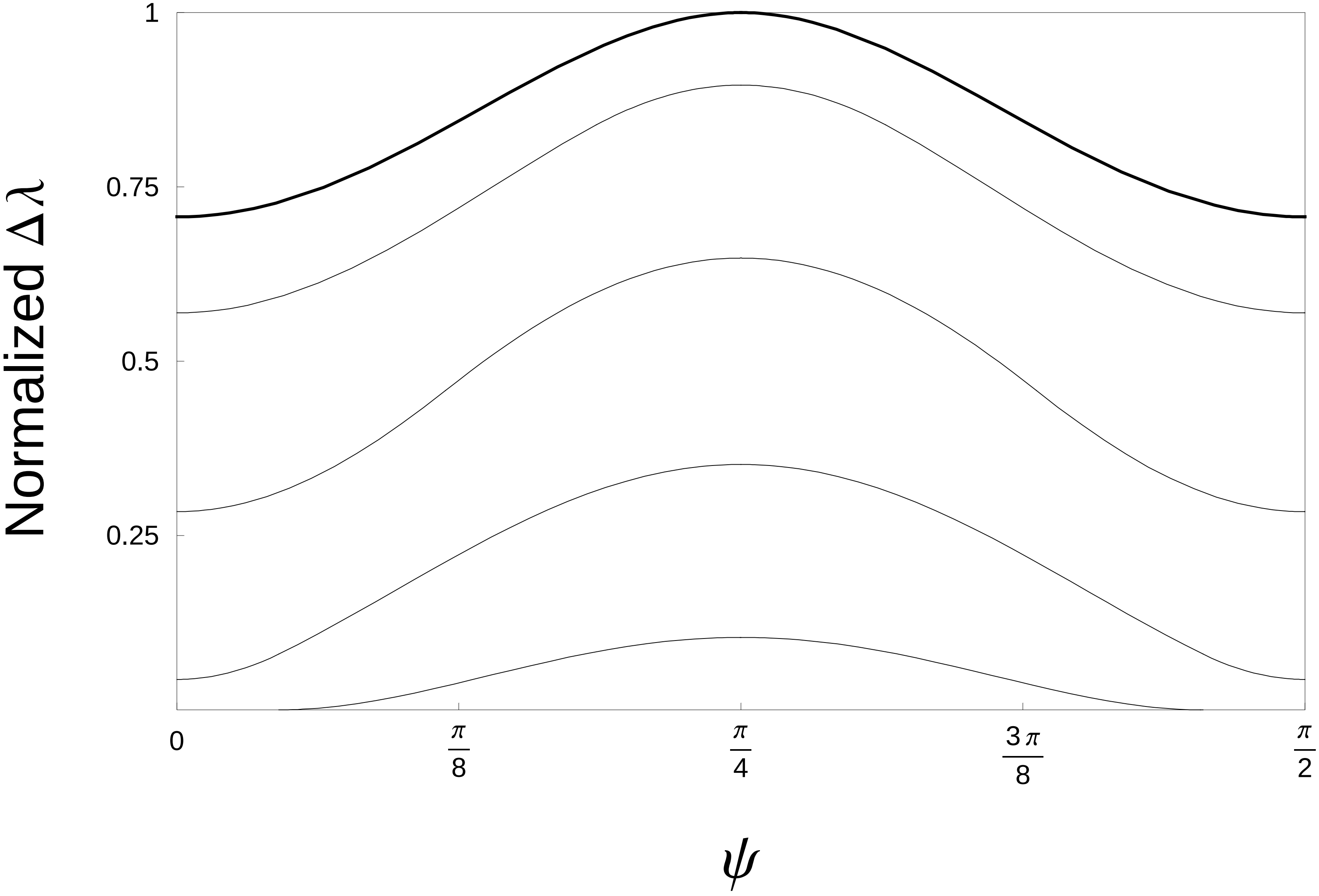

Halterman and Valls Fig.7

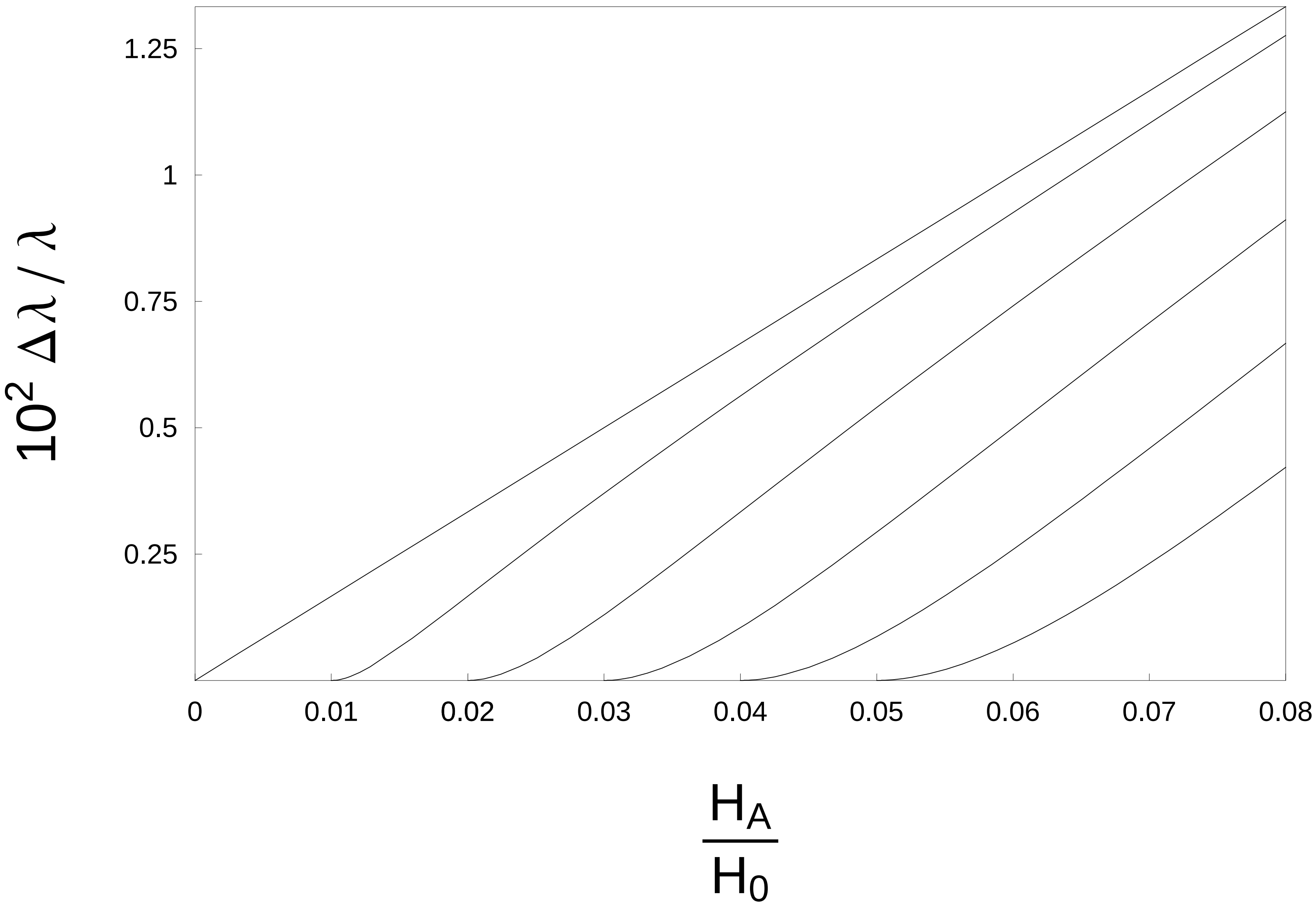

Halterman and Valls Fig.8

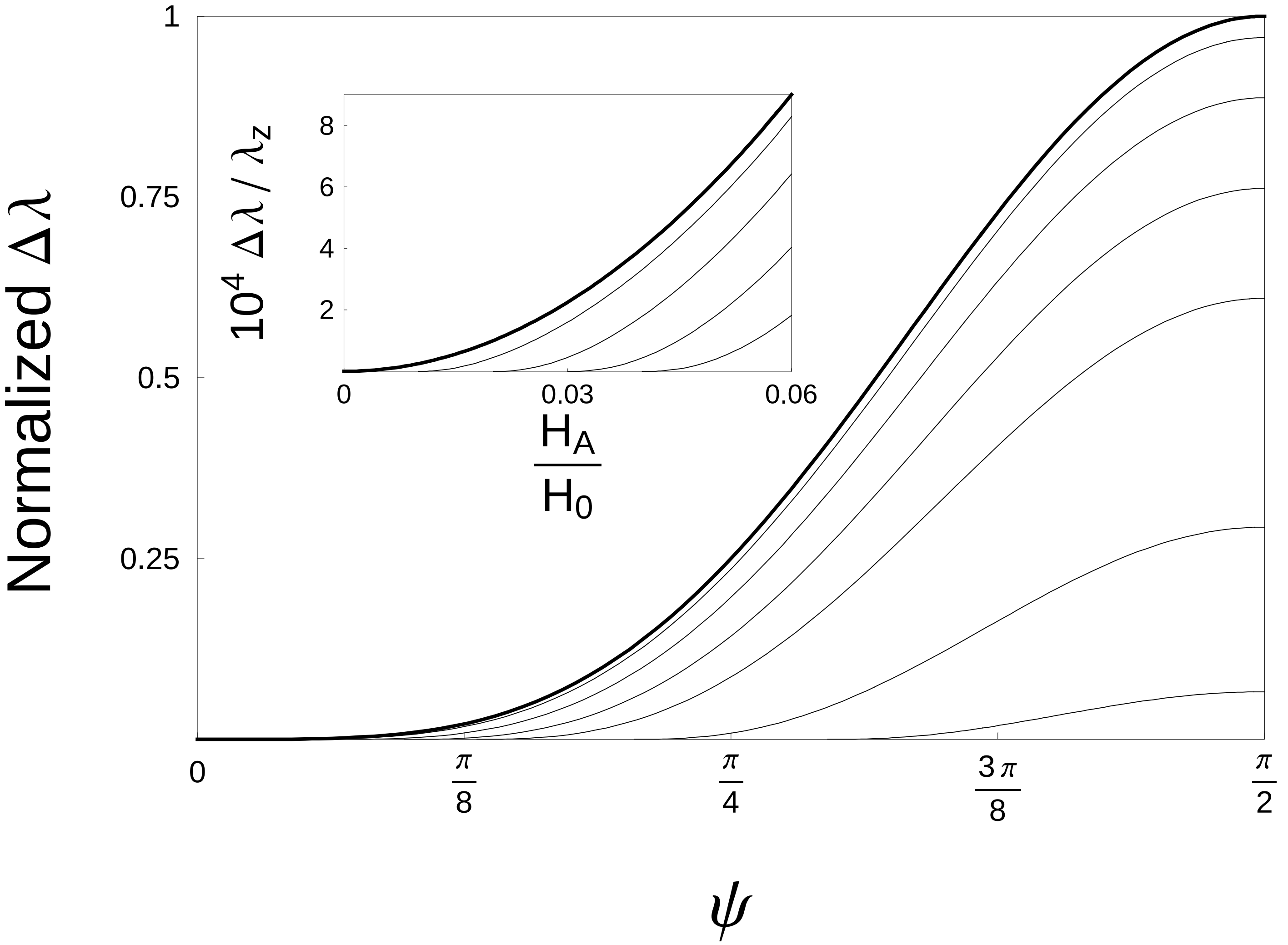

Halterman and Valls Fig.9